

Platinum-group elemental and Sr–Nd–Os isotopic geochemistry of Permian Emeishan flood basalts in Guizhou Province, SW China

Liang Qi*, Mei-Fu Zhou

*Department of Earth Sciences, The University of Hong Kong, Pokfulam Road, Hong Kong SAR, China
State Key Lab of Ore Deposit Geochemistry, Institute of Geochemistry, Chinese Academy of Sciences, Guiyang, 550002, China*

Received 5 May 2006; received in revised form 14 November 2007; accepted 17 November 2007

Editor: S.L. Goldstein

Abstract

The 260 Ma Emeishan continental flood basalts (ECFB) occur in SW China and northern Vietnam. A 550-m-thick sequence of ECFB in Guizhou Province (SW China) is composed of 12 basaltic lava flows, each ranging from 10 to 140 m in thickness. All samples belong to the high-Ti basalts ($\text{TiO}_2 = 1.9\text{--}4.4$ wt.% and $\text{Ti}/\text{Y} = 400\text{--}700$). Relative to the upper flows (Flows 9–12), those from the lower part of the section (Flows 1–8) are depleted in Nb, Ta, P and Sr and enriched in Zr, La and Th, consistent with higher degree of crustal contamination. Overall, the concentrations of Os, Ir and Ru range from 0.01 to 0.23 ppb and are low relative to those of Rh, Pt and Pd, which range from 0.2 to 1.1, 6 to 17 and 5 to 18 ppb, respectively. Different lava flows have different primitive mantle-normalized PGE patterns, and samples from the same flow show similar patterns. Fractionations between PPGE and IPGE are mainly controlled by olivine and chromite fractionation. The negative correlations between Pd/Ir and Pt/Pd, and Ni/Pd and Pd/Cr are consistent with crystal fractionation. Flows 6–8 and 10–12 show obvious negative Ru anomalies, explained by fractionation of laurite (Ru, Os, IrS_2 or Os–Ir–Ru alloys in the primary magma, or by coprecipitation of laurite with chromite or olivine. Flows 9–12 are Os-poor and have higher initial $^{187}\text{Os}/^{188}\text{Os}$ ratios than Flows 1–8, indicating it is easy to alter the Os isotopic compositions of basaltic magmas with lower Os concentrations.

© 2007 Elsevier B.V. All rights reserved.

Keywords: Basalts; PGE; Re–Os isotopes; Emeishan continental flood basalts; SW China

1. Introduction

The Emeishan continental flood basalts (ECFB) in SW China and northern Vietnam form a major part of the ~260 Ma Emeishan Large Igneous Province (Zhang et al., 1988; Chung and Jahn, 1995; Song et al., 2001; Xu et al.,

2001; He et al., 2003; Xiao et al., 2003; Xu et al., 2004a). The volcanic sequence includes high-Ti and low-Ti basalts (Xu et al., 2001; Xiao et al., 2003) and is associated with a variety of plutonic rocks (Zhong et al., 2002; Zhou et al., 2002a, 2005, 2006). The processes that control the diversity of these igneous rocks are not well understood, although a general model involving mantle plume–lithosphere interaction and crustal contamination has been proposed (Chung and Jahn, 1995; Song et al., 2001; Xu et al., 2001; Xiao et al., 2003). Previous studies were based on major and trace element compositions and

* Corresponding author. Present address: State Key Lab of Ore Deposit Geochemistry, Institute of Geochemistry, Chinese Academy of Sciences, Guiyang, China, 550002.

E-mail address: qiliangku@hotmail.com (L. Qi).

Sr–Nd isotopic data of basaltic rocks in several representative cross-sections in Sichuan and Yunnan Provinces (Song et al., 2001; Xu et al., 2001; Xiao et al., 2003; Xu et al., 2004b).

Magmatism associated with large igneous provinces may show temporal variations, reflecting variable mantle sources and different degrees of mantle plume–lithosphere interaction, crustal contamination, S-saturation and fractional crystallization, or a combination of these processes (Arndt et al., 1993, 1998, 2003; Lightfoot and Keays, 2005). PGE concentrations are known to be sensitive indicators of the degree of partial melting, the nature of the source region, and the extent of sulfide segregation, and thus are important for understanding the petrogenesis of mantle-derived rocks. These elements have been used elsewhere to examine the genetic relationship between continental flood basalts and sulfide mineralization (Brügmann et al., 1993; Wooden et al., 1993; Vogel and Keays, 1997; Maier and Barnes, 1999; Rehkämper et al., 1999; Crocket, 2000; Philipp et al., 2001; Momme et al., 2002; Maier et al., 2003; Momme et al., 2003; Ely and Neal, 2003; Crocket and Paul, 2004; Lightfoot and Keays, 2005). For example, Ir, Pt, Pd and Au concentrations, trace element characteristics and Sr and Nd isotopic ratios of basalts from the Maharashtra region of the Deccan Traps suggest variable mantle sources and different degrees of crustal contamination (Crocket and Paul, 2004). However, low PGE contents in basalts make accurate analysis difficult, resulting in relatively few studies of PGE in such rocks (Rehkämper et al., 1999; Momme et al., 2002, 2003; Lightfoot and Keays, 2005). The only study of the platinum-group elements (PGE) and their temporal variation through ECFB is on the low-Ti basalts in the Northern part of ELIP (Song et al., 2006).

In order to accurately measure low concentrations of PGE in basaltic rocks, we have developed an improved Carius tube analytical method (Qi et al., 2007). Using this method, we have analyzed PGEs in representative basalts collected from a cross-section in the eastern part of the ECFB in Guizhou Province, SW China. In addition, the samples were analyzed for whole-rock major and trace elements. To evaluate the extent of crustal contamination in the ECFB and to understand the processes leading to the formation of the ECFB and its ore deposits, we also measured Sr–Nd isotope compositions and $^{187}\text{Os}/^{188}\text{Os}$ ratios in these samples using ICP-MS. Because the parent–daughter elemental ratios in mafic and felsic rocks show much larger variations in the Re–Os isotopic system compared to the Rb–Sr, Sm–Nd or U–Th–Pb systems, Os isotopes are highly sensitive tracers for the interaction of basaltic melts with the continental crust. We use this

comprehensive dataset to investigate the factors controlling the petrogenesis of the ECFB, mantle melting and subsequent differentiation and crustal contamination.

2. Geological background

The ECFB crops out in the eastern part of the Tibetan Plateau and the western part of the Yangtze Block (Fig. 1). The thickness of the ECFB ranges from several hundred meters to 5 km (Xiao et al., 2003, 2004). The easternmost part of the Tibetan Plateau is the Songpan–Ganze Terrane, which is characterized by a thick (up to more than 10 km) sequence of Late Triassic strata of deep marine origin. The Yangtze Block consists of a Precambrian basement overlain by stratigraphic sequences ranging from Late-Mesoproterozoic to Upper Jurassic and younger in age. The lower and middle parts of the sequence are mainly marine sedimentary rocks, whereas the upper part consists mostly of terrestrial basin deposits (Yan et al., 2003a). Along the western margin of the Yangtze Block there are abundant Neoproterozoic granites and associated metamorphic rocks known as the Kangdian complexes, which were likely uplifted at ca. 175 Ma (Zhou et al., 2002b; Yan et al., 2003b).

In addition to picrites, tholeiites and basaltic andesites of the volcanic sequence, the Emeishan Large Igneous Province contains numerous mafic–ultramafic and syenitic intrusions. In the western part of the ECFB, the volcanic succession has been strongly deformed, uplifted and eroded as a result of the Tertiary India–Eurasia collision (see reviews in Ali et al., 2004). The Middle-Late Permian flood basalts can be traced to the Yidun and Qingtang Terranes to the west (Fig. 1) (Song et al., 2004), and their distribution has been used to suggest that the thick Triassic sequence was deposited in a basin that formed in response to rifting caused by the Emeishan mantle plume (Song et al., 2004). Permian flood basalts also crop out south of the Red River Fault at Jinping in southern Yunnan Province (Xiao et al., 2003) and in the Song Da area of northern Vietnam (Hanski et al., 2004). Flood basalts and related mafic rocks in the Funing area, northeast of the Red River Fault, have also recently been suggested to be part of the ECFB (Zhou et al., 2006). Therefore the true extent of the ECFB might have been under-estimated, perhaps on the order of 1×10^6 km² (Song et al., 2004; Zhou et al., 2006).

Basalts in Heishitou is located in Weining county of the Guizhou Province (Fig. 1). Strata in the Weining area are continuous from the Neoproterozoic to Quaternary except Middle-Upper Ordovician and Upper Silurian. The maximum thickness of ECFB at Weining is about 1229 m. The basalts are unconformably underlain by

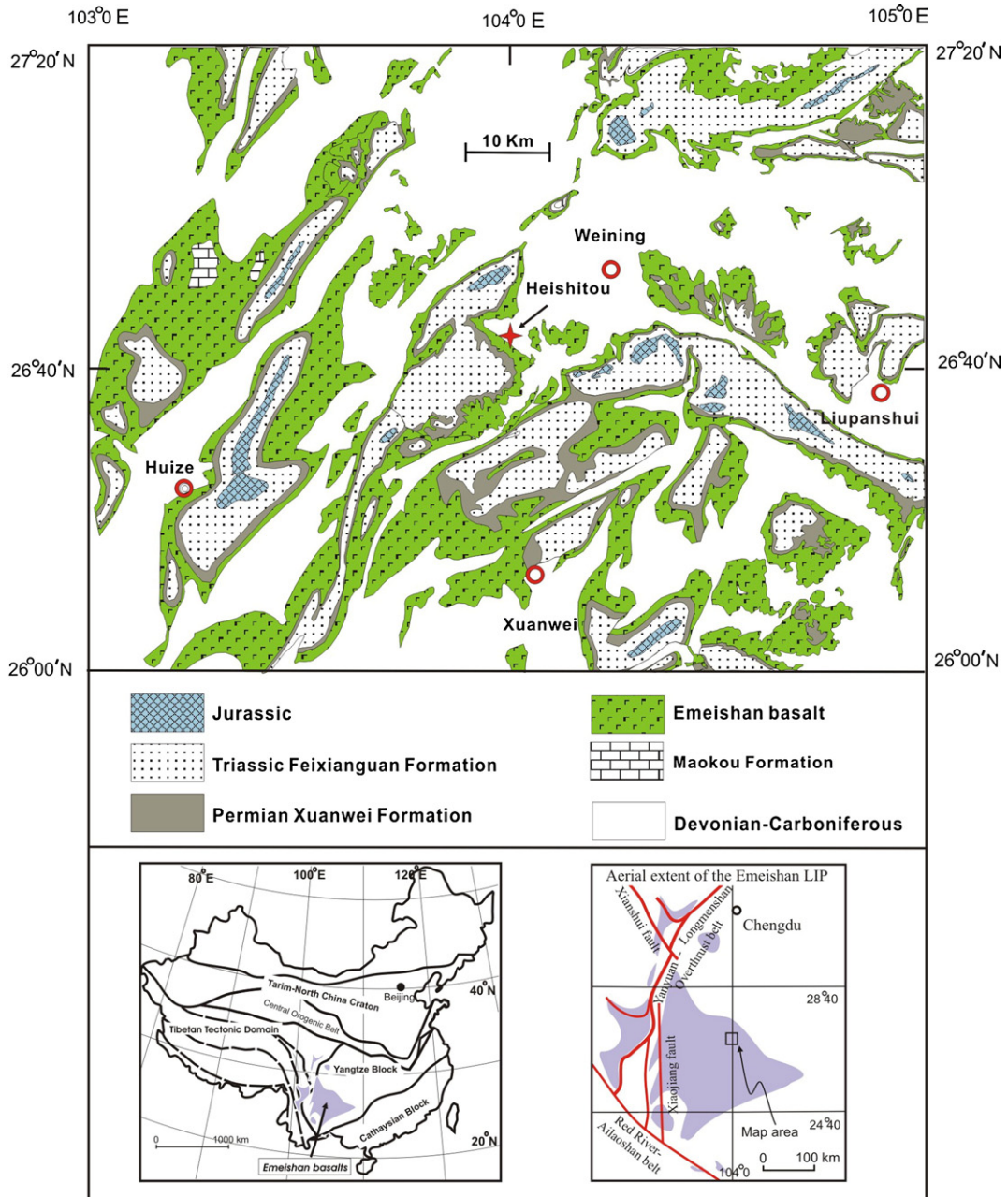



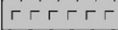
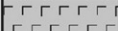
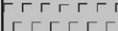


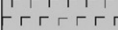
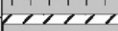

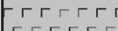

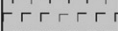
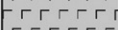
Fig. 1. Geological map of the Western Guizhou Province, SW China, showing the distribution of the Emeishan flood basalts. Note that the area is the easternmost part of the Emeishan Large Igneous Province.

limestones of the Lower Permian Maokou Formation, and are conformably overlain by the Upper Permian Xuanwei Formation composed of sandstone, mudstone and conglomerate with interbedded coal seams.

3. Flood basalts in Heishitou

Basalts in Heishitou are exposed in a relatively well-preserved cross-section, because it has been little

affected by the Tertiary collision between India and Eurasia (Fig. 1). The thickness of the Heishitou sequence is about 550 m with each flow ranging from 10 to 140 m (Fig. 2). Each flow comprises a massive portion with well-developed columnar jointing with breccias and tuffs on the top. They have typical porphyritic and vesicular textures and are composed of plagioclase (55–65 modal%), titanite (30–35 modal%), Fe–Ti oxides (magnetite and ilmenite) (5–10 modal%) and biotite (<5 modal%).

| Late Permian | Xuanwei formation | Thickness (m) | Samples | Column |
|------------------------|-------------------|---------------|----------|---|
| Emeishan flood basalts | Flow-12 | 10 | GZ-66-67 |  |
| | Flow-11 | 20 | GZ-63-65 |  |
| | Flow-10 | 40 | GZ-57-62 |  |
| | Flow-9 | 60 | GZ-51-56 |  |
| | Flow-8 | 50 | GZ-45-49 |  |
| | Flow-7 | 70 | GZ-36-42 |  |
| | Flow-6 | 30 | GZ-32-35 |  |
| | Flow-5 | 40 | GZ-27-30 |  |
| | Flow-4 | 140 | GZ-14-26 |  |
| | Flow-3 | 20 | GZ-9-13 |  |
| | Flow-2 | 30 | GZ-5-8 |  |
| | Flow-1 | 40 | GZ-1-4 |  |
| Middle Permian | Maokou formation | | |  |


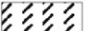
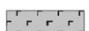
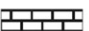
| | | | |
|---|-----------|---|-----------|
|  | Sandstone |  | Tuff |
|  | Basalt |  | Limestone |

Fig. 2. A section showing a sequence of the Emeishan flood basalts at Heishitou, Guizhou Province, SW China. Note that the stratigraphic sequence contains 12 lava flows, each separated by breccias and tuff.

The most common phenocrysts are tabular plagioclase crystals of variable size, locally accompanied by sparse clinopyroxene. The phenocrysts are set in a fine-grained, intergranular to intersertal groundmass composed of plagioclase (25–60 modal%), clinopyroxene (15–30 modal%), partly devitrified basaltic glass (20–45 modal%), and minor Fe–Ti oxides (<5 modal%). Amygdaloidal texture is best developed in the upper parts of the flows, where the vesicles are mostly filled with chlorite. In general, the basalts are fresh with only minor chlorite along fractures.

4. Analytical methods

4.1. Major oxides and trace elements

Samples were cut with a diamond-impregnated brass blade, crushed in a steel jaw crusher that was brushed and cleaned with de-ionized water between samples, and pulverized in agate mortars in order to minimize contamination. Major oxides were determined by wavelength-dispersive X-ray fluorescence spectrometry on fused glass beads using a Philips PW2400 spectrometer at the University of Hong Kong. Trace elements were determined by a VG PQ ExCell inductively-coupled plasma mass spectrometry (ICP-MS) at the University of Hong Kong using the method of [Liang et al. \(2000\)](#). Analytical results and the uncertainties (1σ , $N=5$) of reference materials, AMH-1 (andesite) and OU-6 (slate) are listed in Supplementary Table 1 ([Potts and Kane, 2005](#); [Thompson et al., 2000](#)). The analytical accuracies are estimated to be $\pm 2\%$ (relative) for major oxides present in concentrations greater than 0.5% and $\pm 5\%$ (relative) for minor oxides present in concentrations between 0.1 wt.% and 0.5% (Supplementary Table 1). The accuracies of the ICP-MS analyses are estimated to be better than $\pm 5\%$ (relative) for most elements.

4.2. PGE and Re–Os isotopic compositions

Most of the previous analytical procedures for PGE include Ni-sulfide fire assay combined with Te-coprecipitation (e.g. [Gros et al., 2002](#)), but this technique results in relatively high blanks and loss of Os because of the volatile nature of its oxides. In this study, Re and PGE were measured by isotope dilution (ID)-ICP-MS after digestion of samples using a modified Carius tube technique ([Qi et al., 2007](#)). Twelve grams of rock powder and appropriate amount of enriched isotope spike solution containing ^{185}Re , ^{190}Os , ^{193}Ir , ^{101}Ru , ^{194}Pt and ^{105}Pd were digested with 35 ml *aqua regia* in a 75 ml Carius tube, which was placed in a custom-made high-

pressure autoclave filled with water to prevent explosion of the tube when heated to 330 °C. After 10 h, the Carius tube was cooled and the contents were transferred to a 50 ml centrifuge tube. After centrifuging, the upper solution was transferred to a custom-made distillation system for Os distillation. The collected Os solution was used for measuring the ratios of $^{187}\text{Os}/^{188}\text{Os}$ and $^{192}\text{Os}/^{190}\text{Os}$ by VG PQ ExCell ICP-MS at The University of Hong Kong. After distillation, about 1/4 of the residual solution was used to separate Re from the matrix using AG 1-X8 anion exchange resin. The remainder of the aliquot was used to pre-concentrate PGE by Te-precipitation, as described in Qi et al. (2004).

In our improved Carius tube technique, the usage of a sealed stainless steel high-pressure autoclave filled with water is to prevent explosion of the tube. During heating, the external and internal pressures of the Carius tube increase simultaneously, such that the possible explosion of Carius tube can be avoided. Consequently, this technique allows a higher temperature (up to 330 °C), a greater volume of aqua regia (up to 2/3 of the total volume of the Carius tube) and thus larger sample mass (12 g) relative to the normal Carius tube technique (Shirey and Walker, 1995; Meisel and Moser, 2004). Our experiment demonstrates that pure chromite can be totally dissolved in less than 12 h at 330 °C, indicating this method is more effective than the normal Carius tube technique. This improved method is a low cost and low maintenance approach compared with the HPA-S (high-pressure asher) technique. Low procedure blanks and detection limits make this technique suitable for analyzing PGE of mafic rocks.

Analytical results for standard reference materials, including WPR-1 (peridotite), WGB-1 (gabbro), TDB-1 (diabase) and an in-house standard, EMBA-1 (Emeishan flood basalt), are shown in Table 1. The PGE concentrations for Ru, Rh, and Ir in WGB-1 and TDB-1 are lower

than the recommended values, but agree well with values reported recently (Meisel and Moser, 2004). The results for WPR-1 are in excellent agreement with the certified values. Despite the very low concentrations of Ru, Ir, and Os (less than 0.1 ppb) in the basaltic sample, EMBA-1, our analyses yielded reproducible results (Table 1). The total procedural blanks were lower than 0.002 ng/g for Os; 0.003 ng/g for Re, Ru, Rh and Ir, 0.020 ng/g for Pd, and 0.011 ng/g for Pt. The mass bias effect on Os was monitored by measuring a ~10 ppb natural Os laboratory standard solution between every five samples. The mass bias factors were calculated using the measured $^{188}\text{Os}/^{189}\text{Os}$ values for the standard, the accepted value of $^{188}\text{Os}/^{189}\text{Os}=0.8261$ (IUPAC, 1991), and the exponential fractionation law. These mass bias factors were used to fractionation correct the $^{187}\text{Os}/^{188}\text{Os}$ ratios of the samples following the method described by Schoenberg et al. (2000). This allowed determination of the spike contributions to each measurement. The added ^{187}Os and ^{188}Os from the spike were corrected by calculating the ^{189}Os intensity of the spike following the method described by Qi et al. (2004). Each measurement consisted 20 scans, with intensities of ^{188}Os and ^{189}Os from 50,000 to 60,000 cps for the standard, and 5000 to 10,000 cps for most of the samples. The Os standard solution was measured 12 times during the course of sample analyses and yielded fractionation corrected $^{187}\text{Os}/^{188}\text{Os}=0.136\pm 3$ (2σ). Analytical results of PGEs and the uncertainties of $^{187}\text{Os}/^{188}\text{Os}$ values are listed in Supplementary Table 2.

4.3. Rb–Sr and Sm–Nd isotopic analyses

Isotope ratios of Sr–Nd and concentrations of Rb, Sr, Sm, and Nd were determined on a Finnigan MAT 262 thermal ionization magnetic sector mass spectrometer at The Institute of Geology and Geophysics, CAS, Beijing.

Table 1

Blank (ng), detection limits (DL) (ng/g) and analytical results (ng/g) of reference materials, WGB-1, TDB-1, WPR-1 and in-house standard EMBA-1

| Elements | Blank | DL (3 σ) | WGB-1 (Gabbro) | | | | TDB-1 (Diabase) | | | | WPR-1 (Peridotite) | | EMBA-1 (Basalt) | | |
|----------|--------|---------------------|-------------------|----------|--------|-----------|-----------------|----------|--------|-----------|--------------------|-----------|-----------------|----------|--|
| | | | Average N=6 | RSD % | Meisel | Certified | Average N=6 | RSD % | Meisel | Certified | Average N=6 | Certified | Average N=6 | RSD % | |
| Re | 0.026 | 0.002 | 1.14±0.01 | 1.3 | 1.15 | | | | | | | | | | |
| Os | 0.0026 | 0.0002 | 0.37±0.02 | 5.1 | 0.544 | | | | | | | | | | |
| Ir | 0.025 | 0.001 | 0.16±0.02 | 13.5 | 0.211 | 0.33 | | | | | | | | | |
| Ru | 0.017 | 0.001 | 0.13±0.01 | 11.5 | 0.144 | 0.3 | | | | | | | | | |
| Rh | 0.026 | 0.001 | 0.20±0.02 | 9.7 | 0.234 | 0.32 | | | | | | | | | |
| Pt | 0.18 | 0.009 | 6.34±0.61 | 10.1 | 6.39 | 6.1 | | | | | | | | | |
| Pd | 0.37 | 0.015 | 13.0±1.1 | 7.3 | 13.9 | 13.9 | | | | | | | | | |

Meisel = (Meisel and Moser, 2004); Certified = (Govindaraju, K., 1994).

The chemical separation and isotopic measurement procedures are described in Zhang et al. (2001). Mass fractionation corrections for Sr and Nd isotopic ratios were based on values of $^{86}\text{Sr}/^{88}\text{Sr}=0.1194$ and $^{146}\text{Nd}/^{144}\text{Nd}=0.7219$. Uncertainties in Rb/Sr and Sm/Nd ratios are less than $\pm 2\%$ and $\pm 0.5\%$ (relative), respectively. The Sr standard solutions (NBS 987) were analyzed 8 times and yield a $^{87}\text{Sr}/^{86}\text{Sr}$ ratio of 0.710237 ± 25 (2σ), whereas the Nd standard solutions (Ames) which is the same as used by Roddick et al. (1992) were also analyzed 8 times and have an $^{143}\text{Nd}/^{144}\text{Nd}$ ratio of 0.512139 ± 15 (2σ) during the period of data acquisition. The result for Ames Nd is comparable with the published data of 0.512147 ± 7 which is calibrated to a LaJolla value of 0.511862 ± 8 (2σ) (Roddick et al., 1992) and 0.512125 ± 10 (Chen et al., 2002). The measured results for USGS standard BCR-1 were Rb 45.49 ppm, Sr 340.0 ppm, $^{87}\text{Sr}/^{86}\text{Sr}$ 0.704995 ± 25 (2σ) and Sm 6.59 ppm, Nd 28.8 ppm and $^{143}\text{Nd}/^{144}\text{Nd}$ 0.512638 ± 16 (2σ), which are comparable with the published data of Rb 46.54 ppm, Sr 329.5 ppm,

$^{87}\text{Sr}/^{86}\text{Sr}$ 0.705027 ± 74 (2σ) and Sm 6.676 ppm, Nd 28.77 ppm and $^{143}\text{Nd}/^{144}\text{Nd}$ 0.512633 ± 35 (2σ) (Chen et al., 2007). The results of Sr and Nd standard solutions and reference materials are listed in Table 2.

5. Analytical results

5.1. Major and trace elements

Samples from Heishitou are all basaltic in composition with SiO_2 ranging from 44 to 51 wt.%, MgO from 4 to 6 wt.% and Mg# from 33.4 to 48.4 (Supplementary Table 1). All of the analyzed samples have TiO_2 contents of 1.9–4.4 wt.% and Ti/Y ratios of 400–700 and belong to the high-Ti basalt group (Xu et al., 2001). There are slightly different geochemical features between samples in the lower part of the section (Flows 1–8) and in the upper part (Flows 9–12). Samples from Flows 1–8 have notably higher TiO_2 (3.6–4.4 wt.%) than those from Flows 9–12 (2.0–3.9 wt.%). Many incompatible elements, such as TiO_2 , P_2O_5 , La, Th, Nb and Zr,

Table 2
Rb–Sr and Sm–Nd elemental and isotopic analyses of Heishitou basalts, Guizhou Province, SW China

| Flow | Sample | Rb (ppm) | Sr (ppm) | $^{87}\text{Rb}/^{86}\text{Sr}$ | $^{87}\text{Sr}/^{86}\text{Sr}\pm 2\sigma$ | $(^{87}\text{Sr}/^{86}\text{Sr})_i$ | Sm (ppm) | Nd (ppm) | $^{147}\text{Sm}/^{144}\text{Nd}$ | $^{143}\text{Nd}/^{144}\text{Nd}\pm 2\sigma$ | $(^{143}\text{Nd}/^{144}\text{Nd})_i$ | ϵ_{Nd} |
|---------|---------------------------|-------------|-------------|---------------------------------|--|-------------------------------------|-------------|-------------|-----------------------------------|--|---------------------------------------|------------------------|
| Flow 1 | GZ-2 | 32.3 | 473.2 | 0.1972 | 0.707331 ± 12 | 0.706602 | 10.72 | 51.63 | 0.1256 | 0.512519 ± 12 | 0.512305 | 0.03 |
| Flow 2 | GZ-6 | 47.4 | 804.5 | 0.1703 | 0.707085 ± 11 | 0.706455 | 10.90 | 51.35 | 0.1283 | 0.512585 ± 12 | 0.512367 | 1.24 |
| Flow 3 | GZ-10 | 46.9 | 477.7 | 0.2842 | 0.707316 ± 13 | 0.706265 | 11.20 | 52.77 | 0.1283 | 0.512584 ± 13 | 0.512366 | 1.22 |
| Flow 4 | GZ-18 | 33.9 | 470.1 | 0.2087 | 0.706418 ± 11 | 0.705646 | 10.67 | 48.44 | 0.1331 | 0.512650 ± 13 | 0.512423 | 2.35 |
| Flow 5 | GZ-28 | 34.5 | 497.3 | 0.2005 | 0.706247 ± 13 | 0.705505 | 10.41 | 47.96 | 0.1313 | 0.512651 ± 13 | 0.512428 | 2.43 |
| Flow 6 | GZ-33 | 34.6 | 492.1 | 0.2032 | 0.705964 ± 11 | 0.705213 | 10.50 | 47.81 | 0.1327 | 0.512654 ± 12 | 0.512428 | 2.43 |
| Flow 7 | GZ-39 | 22.1 | 532.0 | 0.1200 | 0.706076 ± 13 | 0.705633 | 12.03 | 56.59 | 0.1285 | 0.512630 ± 12 | 0.512412 | 2.12 |
| Flow 8 | GZ-47 | 6.10 | 839.8 | 0.0210 | 0.706060 ± 12 | 0.705983 | 10.65 | 50.49 | 0.1275 | 0.512628 ± 13 | 0.512412 | 2.11 |
| Flow 9 | GZ-54 | 3.34 | 279.8 | 0.0345 | 0.706269 ± 13 | 0.706141 | 4.66 | 19.44 | 0.1450 | 0.512533 ± 12 | 0.512286 | −0.33 |
| Flow 10 | GZ-60 | 10.2 | 406.2 | 0.0728 | 0.705133 ± 13 | 0.704863 | 7.67 | 35.40 | 0.1310 | 0.512593 ± 12 | 0.512370 | 1.31 |
| Flow 11 | GZ-64 | 11.4 | 316.3 | 0.1045 | 0.705764 ± 13 | 0.705378 | 9.93 | 47.75 | 0.1258 | 0.512614 ± 14 | 0.512400 | 1.89 |
| Flow 12 | GZ-66 | 7.21 | 594.1 | 0.0351 | 0.705169 ± 12 | 0.705039 | 5.90 | 37.39 | 0.0953 | 0.512654 ± 11 | 0.512492 | 3.68 |
| | Ames (<i>n</i> =8) | | | | | | | | | 0.512139 ± 15 | | |
| | NBS-987 (<i>n</i> =8) | | | | 0.710237 ± 25 | | | | | | | |
| | BCR-1 | 45.49 | 340.0 | | 0.704995 ± 25 | | 6.54 | 28.18 | | 0.512634 ± 16 | | |

Initial isotopic ratios calculated at 260 Ma.

correlate negatively with SiO_2 in Flows 9–12 but not in Flows 1–8 (Fig. 3). Similarly, MgO contents correlate negatively with concentrations of TiO_2 , P_2O_5 , Eu, Cr, Nb and Zr in Flows 9–12 but not in Flows 1–8 (Fig. 4). Flow 9 has wide ranges in major oxides with TiO_2 , Fe_2O_3 , P_2O_5 and K_2O decreasing and Al_2O_3 , MgO and CaO increasing upward (Supplementary Table 1, Fig. 5a). This flow also has higher Cr (117–225 ppm) and Ni (55–84 ppm) than Flows 1–8 and 10–12 (23–78 and 36–65 ppm, respectively).

The Zr/Nb and Th/Ta ratios decrease systematically upwards from Flow 1 to Flow 12 (Fig. 5a), except for three samples in Flow 9. Most elemental ratios in Flow 9,

such as Zr/Nb, Ti/Y, Cu/Zr and Cu/Pd, are distinctly different from ratios in other flows (Fig. 5a and b). Samples from Flow 9 also have lower Zr, Nb, Sr and La, Zr/Y, Ti/Y and Cu/Pd ratios and higher Zr/Nb and Cu/Zr ratios than those from other flows. Zr correlates positively with La and Nb in all the flows (Fig. 6). Samples from the lower and upper parts of the section are distinctly different in plots of Th/Nb vs. Sm/Yb and La/Yb (Fig. 6). All samples have similar chondrite-normalized REE patterns with variable enrichment of light REE (LREE) (Fig. 7). Likewise all samples have similar primitive mantle-normalized trace element patterns (Fig. 8) showing enrichment in large ion lithophile elements (LILE), such

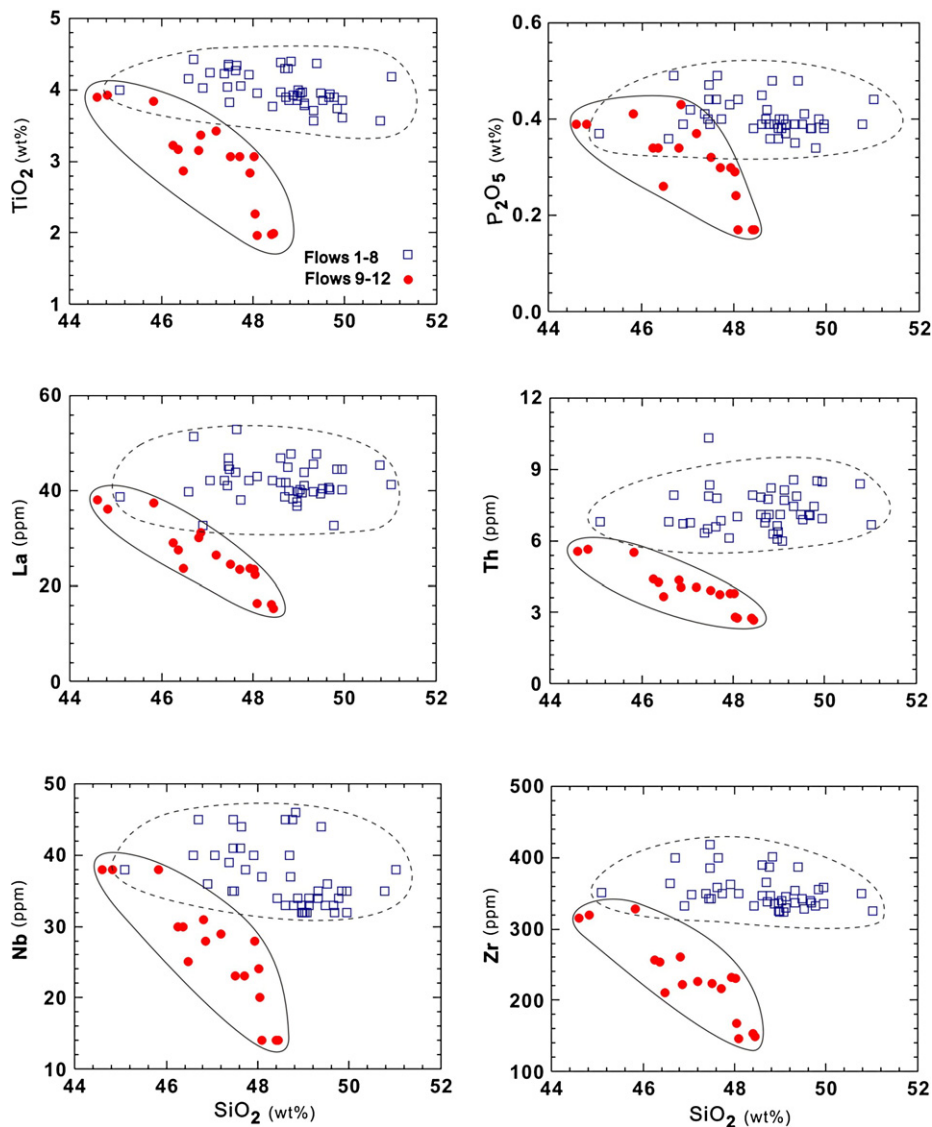


Fig. 3. Harker diagrams showing the variations of SiO_2 vs. major oxides for Heishitou basalts.

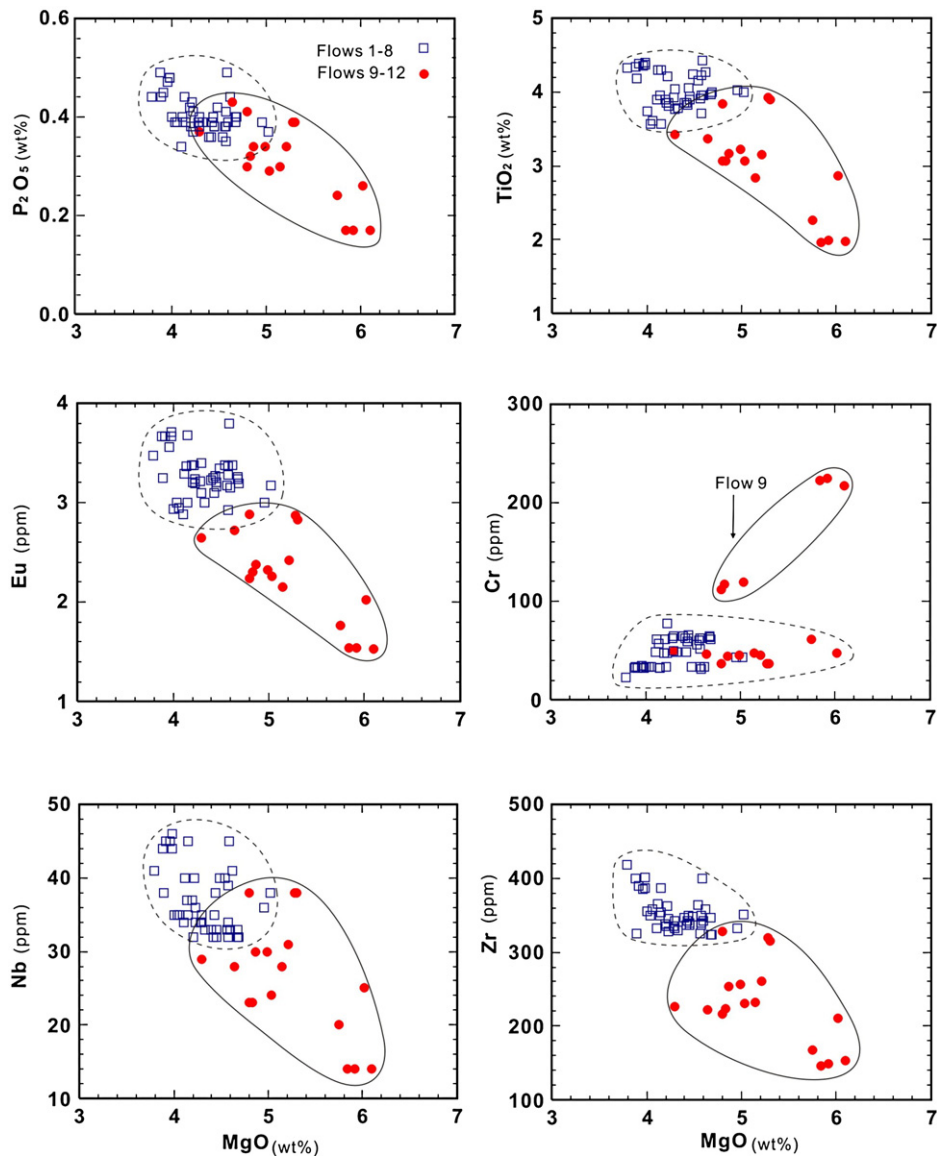


Fig. 4. Plots of MgO vs. other oxides and selected trace elements for Heishitou basalts.

as Ba, Th and U, and negative P anomalies. Samples from Flows 1 to 4 also have weak negative Rb anomalies, whereas Flows 5–12 show strong negative Rb anomalies. Compared with Flows 9–12, samples from Flows 1–8 show weak negative Nb anomalies (Fig. 8).

5.2. Cu, Ni and PGEs

Iridium values vary widely from 0.02 to 0.25 ppb. Flow 9 has the lowest Ir and highest Ru and is easily distinguished from the other flows (Figs. 5b and 9). The Pd/Ir and Pt/Pd ratios correlate negatively whereas a plot of Ni/Pd vs. Pd/Cr (Fig. 9) shows no consistent pattern.

All samples are depleted in Ir-subgroup PGE (IPGE: Os, Ir and Ru) in a primitive mantle-normalized chalcophile element diagram (Fig. 10). Different flows have slightly different patterns, but all samples from the same flow have similar patterns. All samples show enrichment of Cu relative to Ni and PGE. Rocks in Flow 1 have the lowest PGE contents, whereas those in Flow 9 have the highest Cr and Ru contents. Flow 8 has the highest Os (Fig. 5b). Other flows show negative Ru anomalies on primitive mantle-normalized diagrams.

Flows 1–3 and 5–8 have the highest Pt/Pd ratios (0.98–1.76; 0.9–2.12, respectively), while samples from Flows 4 and 9 have the lowest Pt/Pd ratios

(0.54–1.26, respectively). Flows 10–12 have moderate Pt/Pd ratios (0.55–1.29) (Supplementary Table 2, Fig. 5b).

5.3. Re–Os isotopic compositions

The concentration of Re ranges from 0.1 to 1.0 ppb in most samples, except in samples GZ-42 (4.44 ppb), GZ-53 (1.46 ppb) and GZ-55 (2.88 ppb) with high $^{187}\text{Os}/^{188}\text{Os}$ ratios of 1.29, 1.08 and 2.78, respectively (Supplementary Table 2). The Os contents vary from 0.011 to 0.099 ppb for most samples. Flow 8 has the highest Os of all flows ranging from 0.15–0.22 ppb.

The $^{187}\text{Os}/^{188}\text{Os}$ ratios of Heishitou range from 0.17 to 2.78. In Flow 1, the $^{187}\text{Os}/^{188}\text{Os}$ ratios from 0.63 to 0.93, notably higher than in Flows 2 to 8 (0.17–0.63). Flows 9 to 12 have even higher $^{187}\text{Os}/^{188}\text{Os}$ ratios (mostly 0.5–1.0). The highest $^{187}\text{Os}/^{188}\text{Os}$ ratios occur in the samples with the highest Re (GZ-42, GZ-53, and GZ-55) (Supplementary Table 2).

The initial ($^{187}\text{Os}/^{188}\text{Os}$)_i ratios were calculated using the well-constrained age of 260 Ma for the ECFB (Zhou et al., 2002a) and the Re and Os concentrations measured by ICP-MS. Samples with high Os contents have relatively low and constant initial ($^{187}\text{Os}/^{188}\text{Os}$)_i ratios, whereas samples with low Os contents have relatively high and variable ($^{187}\text{Os}/^{188}\text{Os}$)_i ratios (Fig. 11, Supplementary Table 2).

5.4. Rb–Sr and Sm–Nd isotopic compositions

Sm–Nd isotopic compositions of the Heishitou rocks are relatively constant with $^{143}\text{Nd}/^{144}\text{Nd}$ ratios ranging from 0.51252 to 0.5127 and $\varepsilon_{\text{Nd}(t)}$ values ranging from –0.33 to +3.68, whereas the initial $^{87}\text{Sr}/^{86}\text{Sr}$ ratios vary widely from 0.7051 to 0.7073 (Table 2). The $\varepsilon_{\text{Nd}(t)}$ values of the rocks in the lower part of the section are lower than those in the upper part. The $\varepsilon_{\text{Nd}(t)}$ values and Sr ratios of all samples are within the range of the ECFB from previous studies (Fig. 12).

6. Discussion

6.1. Crustal contamination

Because crustal rocks are in general rich in Zr and Th relative to Nb and Ta (Pearce et al., 1984), gradually decreasing Zr/Nb, Th/Nb and Th/Ta ratios from the base to the top of the Heishitou sequence, except for Flow 9 (Fig. 5a) can be explained by decreasing degrees of contamination. The earliest magmas may have been contaminated by disruption and erosion of wall-rock during formation of a magma chamber, whereas the later magmas

may have passed more directly to the surface. However, samples from Flows 1–8 have only slightly negative Nb–Ta anomalies, suggesting only slight contamination.

The degree of crustal contamination of the magmas can be illustrated using $(\text{Nb}/\text{Th})_{\text{PM}}$ and $(\text{Th}/\text{Yb})_{\text{PM}}$ ratios where the rock values have been normalized to the relevant trace element contents of the primitive mantle. $(\text{Nb}/\text{Th})_{\text{PM}}$ is best used to indicate the extent of Nb anomaly whereas $(\text{Th}/\text{Yb})_{\text{PM}}$ is a sensitive indicator of crustal contamination. Samples from Flows 1–8 have lower $(\text{Nb}/\text{Th})_{\text{PM}}$, but higher $(\text{Th}/\text{Yb})_{\text{PM}}$ ratios than Flows 9–12, consistent with a higher degree of crustal contamination (Fig. 13).

During the evolution of the Earth's mantle and development of the crust, Os was preferentially retained in the mantle, whereas Re was moderately enriched in most crustal rocks. Because Os is compatible but Re is moderate incompatible during partial melting, most crustal materials have very low Os abundances and high Re/Os ratios which yield extremely radiogenic Os isotopic signatures (Palmer and Turekian, 1986; Palmer et al., 1988; Koide et al., 1991; Esser and Turekian, 1993). Therefore, minor amounts of crustal contamination will alter significantly the Os isotopic composition of a basaltic magma with low Os concentrations (Reisberg et al., 1993; Widom and Shirey, 1996; Widom et al., 1999).

The high $^{187}\text{Os}/^{188}\text{Os}$ ratios are attributed to crustal contamination and radiogenic ^{187}Os . To evaluate the degree of the crustal contamination in the ECFB, it is necessary to first calculate the contribution of radiogenic ^{187}Os .

The $^{187}\text{Os}/^{188}\text{Os}$ ratio for primitive mantle material is 0.1290 ± 0.0009 (Meisel et al., 1996). Thus, initial $^{187}\text{Os}/^{188}\text{Os}$ ratios in excess of this value are taken as indicators of crustal contamination. In Flows 1–8, the average initial $^{187}\text{Os}/^{188}\text{Os}$ ratios and Os contents are 0.18 and 0.072 ppb, while in Flows 9–12 are 0.28 and 0.025 ppb (Supplementary Table 2). The coupling between low Os contents and high initial $^{187}\text{Os}/^{188}\text{Os}$ ratios indicate that it is easy to alter the Os isotopic compositions of basaltic magmas with low Os concentrations.

6.2. Mantle source and partial melting

Understanding the petrogenesis of basaltic magmas involves estimating their source compositions, degrees of partial melting, and the processes that took place during their ascent and eruption. The degree of partial melting is difficult to estimate because the source compositions are unknown.

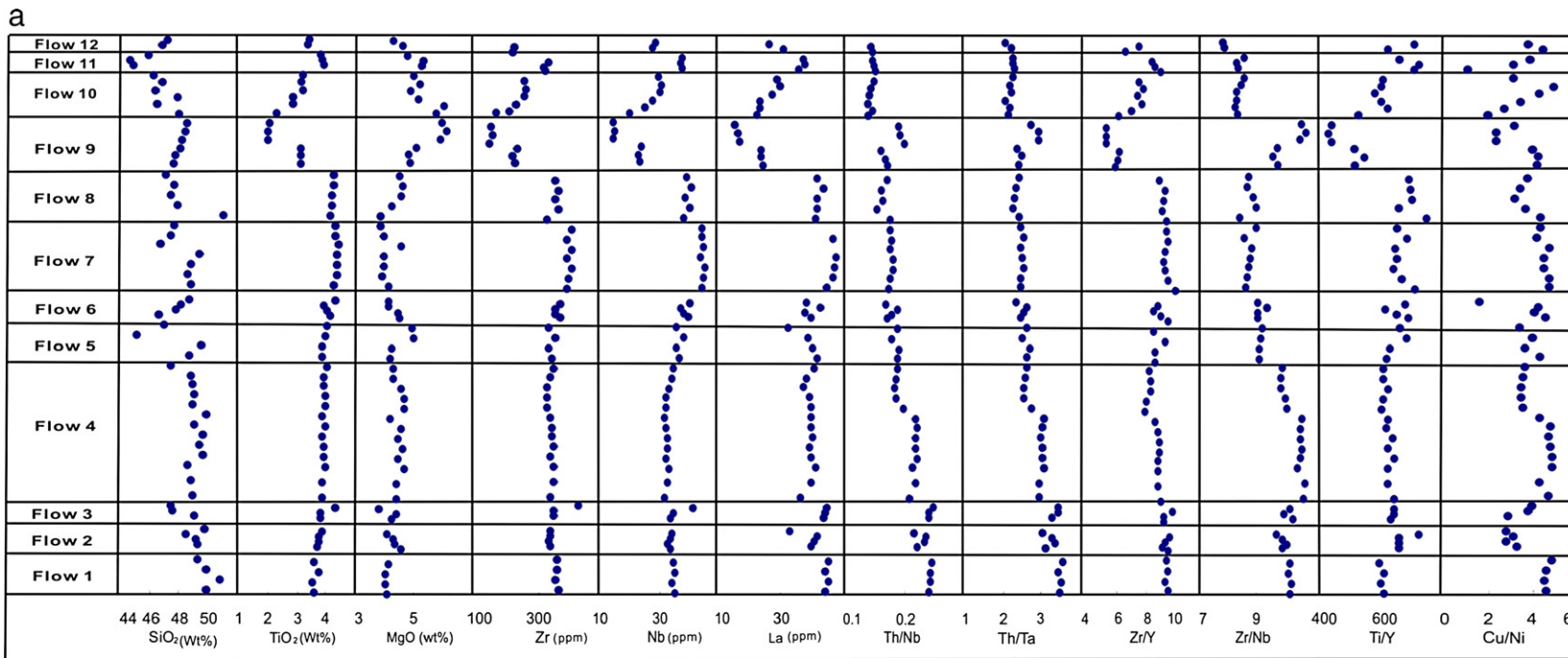


Fig. 5. Compositional variation of Heishitou basalts as a function of stratigraphic position; a) major oxides and trace elements and ratios showing the variations for Heishitou flood basalts and b) Re and PGEs and ratios showing the variations for Heishitou flood basalts.

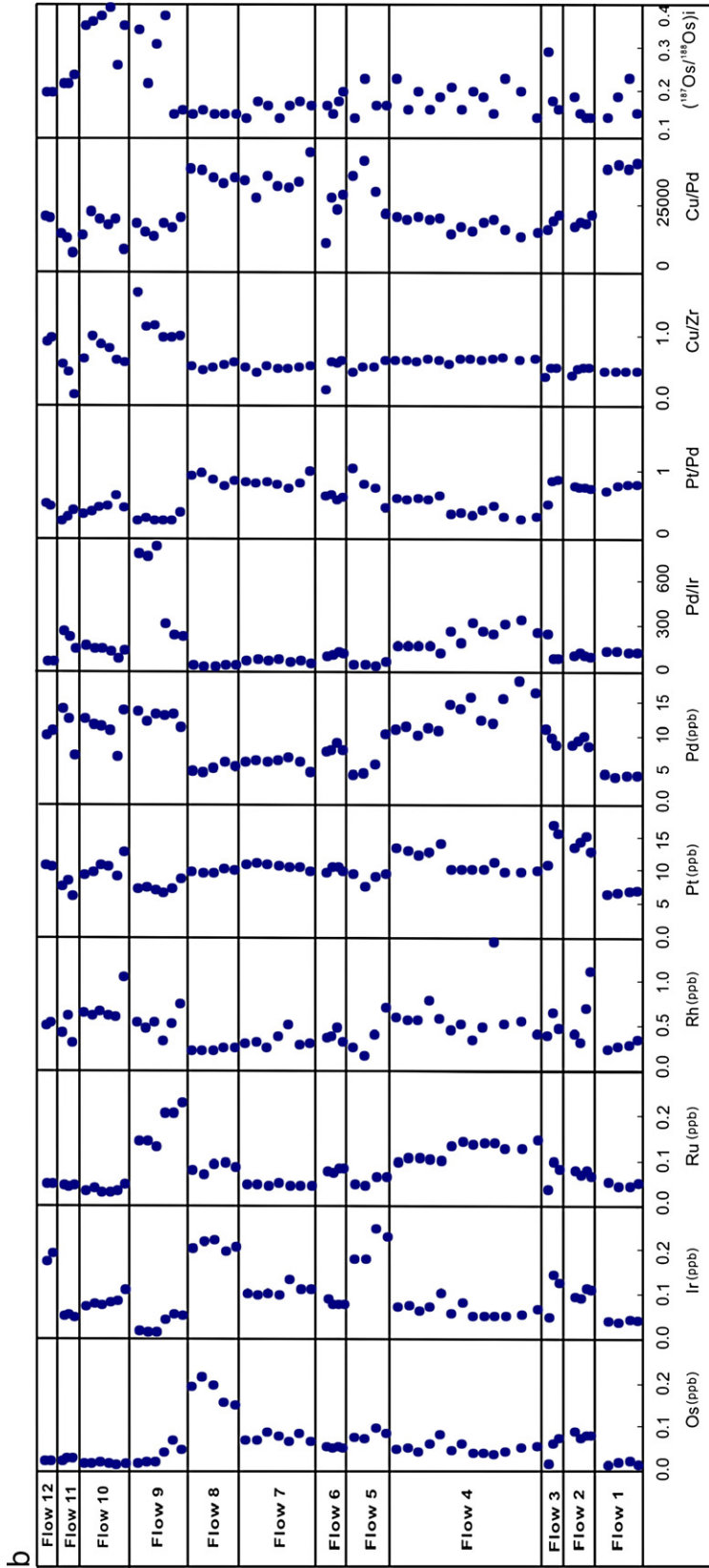


Fig. 5 (continued).

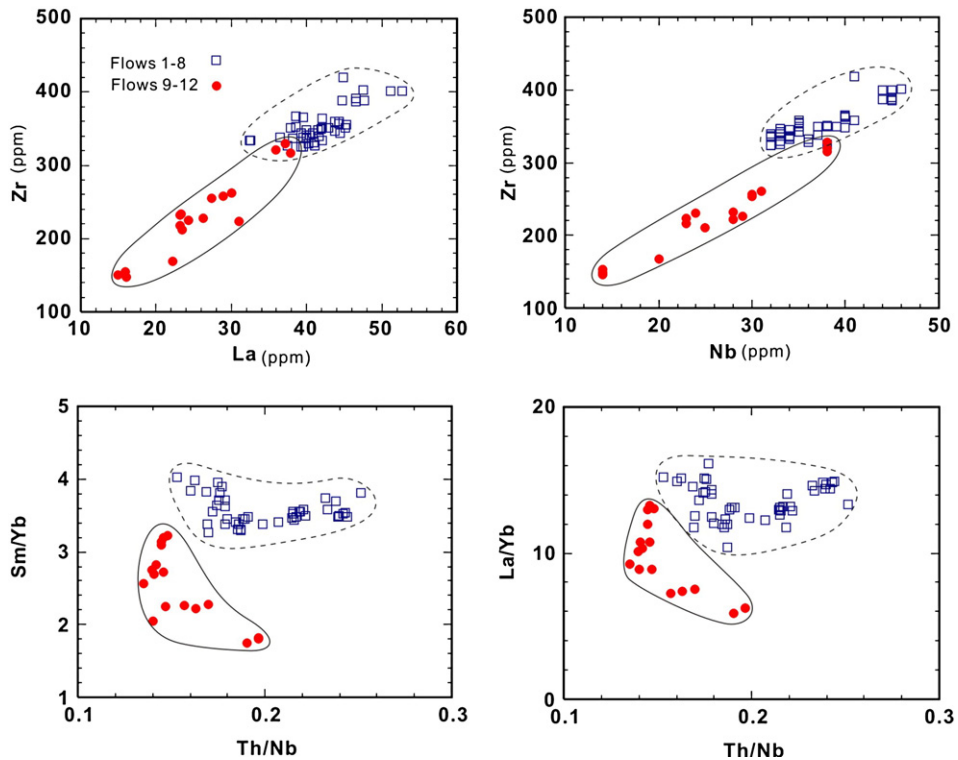


Fig. 6. Plots of Zr vs. La, Zr and Nb, Sm/Yb vs. Th/Nb, and La/Yb vs. Th/Nb for Heishitou basalts.

All Heishitou basalts are rich in Nb and Ta, despite some modification due to crustal contamination. High Nb and Ta contents imply that the high-Ti basalts from Heishitou were derived from an OIB-type mantle source (e.g. Edwards et al., 1994).

Both the composition of the mantle source and degree of partial melting that produced the parental magmas can be estimated using REE abundances and ratios of the basalts. Because Sm and Yb have similar partition coefficients between the melting and the residua, partial melting of a spinel–lherzolite source will result in a constant Sm/Yb ratio, whereas the La/Sm ratio should decrease and the Sm content increase with increasing degrees of melting (Aldanmaz et al., 2000). Therefore, partial melts derived from spinel–lherzolite sources should define melting trends sub-parallel to, and nearly coincident with, a spinel–lherzolite melting trend defined by depleted and enriched source compositions (Green, 2006).

On the other hand, garnet has a high partition coefficient for Yb ($D_{\text{garnet/melt}}=6.6$) relative to Sm ($D_{\text{garnet/melt}}=0.25$) (Johnson, 1998), thus residual garnet in the source will cause a significant increase in the Sm/Yb ratio of the melt. Accordingly, partial melting of garnet–lherzolite mantle with residual garnet will produce a more steeply sloping

trend on a Sm/Yb vs. Sm diagram than melting of a spinel–plagioclase lherzolite source (Fig. 14a). The basalts from Heishitou have Sm/Yb ratios somewhat higher than the spinel–lherzolite melting curve, but lower than those of the garnet–lherzolite melting trend (Fig. 14a, b). Because minor crustal contamination will enhance the Sm/Yb and La/Sm ratios, the original melts from which these samples were derived should plot close to garnet–lherzolite melting curve, implying a garnet lherzolite mantle source.

All Heishitou basalts contain high TiO_2 (1.9–4.4 wt.%) with high Ti/Y ratios (400–700) (Supplementary Table 1 and Fig. 5a) and they belong to the high-Ti group of the ECFB. Garnet has a high partition coefficient for Y ($D_{\text{garnet/melt}}=3.1$) relative to Ti ($D_{\text{garnet/melt}}=0.29$) (Johnson, 1998). The high Ti/Y ratios are thus an indication of a mantle source at a garnet-stable depth.

Different degrees of partial melting will change the melt composition (Gurenko and Chaussidon, 1995), but will not change the isotopic ratios or the ratios of the most incompatible elements. Different basaltic flows in Heishitou have variable isotope and trace element ratios, indicating that their differences in composition primarily reflect different degrees of partial melting.

All of the Heishitou basalts have $\epsilon_{\text{Nd}(t)}$ values ranging from -0.33 to $+3.68$ and different trace element ratios,

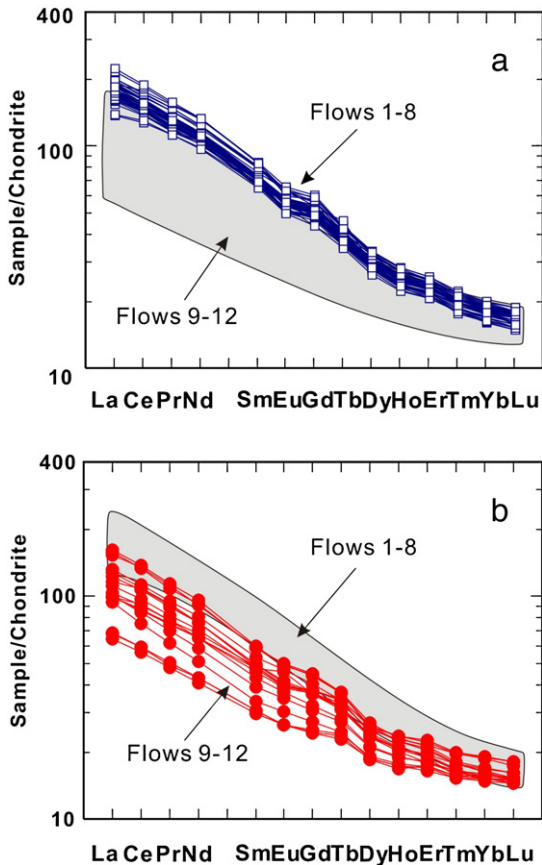


Fig. 7. Chondrite-normalized REE patterns for the flood basalts in Heishitou. The chondrite values are from Sun and McDonough (1989).

indicating that their differences in composition primarily reflect different degrees of partial melting. Flows 9–12 have generally lower TiO_2 (1.9–3.9 wt.%) than Flows 1–8 (3.6–4.4 wt.%). High degrees of partial melting of a mantle source are implied by low abundances of incompatible elements, especially REE, Zr, Hf, Y, Nb and Ta, and of major elements such as TiO_2 and P_2O_5 . High degrees of partial melting will also produce relatively high concentrations of MgO , Ir, Ni and Cr, whereas low degrees of partial melting will produce magmas enriched in incompatible HFSE. Plots of TiO_2 , P_2O_5 , La, Th, Eu, Zr, Nb and Cr versus SiO_2 and MgO (Figs. 3 and 4) show two trends. Flows 1–8 have relatively high and constant contents of these elements, whereas Flows 9–12 have relatively low contents and the elements correlate negatively with SiO_2 and MgO . These observations clearly suggest that Flows 9–12 were derived from magmas formed by higher degrees of partial melting than those that produced Flows 1–8.

Our calculations on trace elements geochemistry suggest that Flows 9–12 formed from melts underwent

about 20% partial melting of the source (Fig. 14a and b). Relatively high degrees of partial melting is also supported by low contents of HFSE and $(\text{La}/\text{Yb})_{\text{PM}}$ ratios of these rocks, which range from 2.61 to 6.83.

6.3. Implications for PGE fractionation

6.3.1. Fractionation of IPGE and PPGE

PGE are traditionally subdivided into compatible IPGE (Os, Ir and Ru) and incompatible PPGE (Rh, Pd and Pt) elements during fractionation of mafic magma. Experiments have confirmed that there is only a slight difference in partition coefficients of individual PGE between sulfide and silicate melts (Bezmen et al., 1994). Thus, removal of sulfide liquid from magma cannot explain the steeply positively-sloped primitive mantle-normalized patterns for the Heishitou basalts (Fig. 10).

It has been suggested that low degrees of partial melting produce a PPGE-rich melt with a high Pd/Ir ratio, whereas higher degrees of melting produce magmas

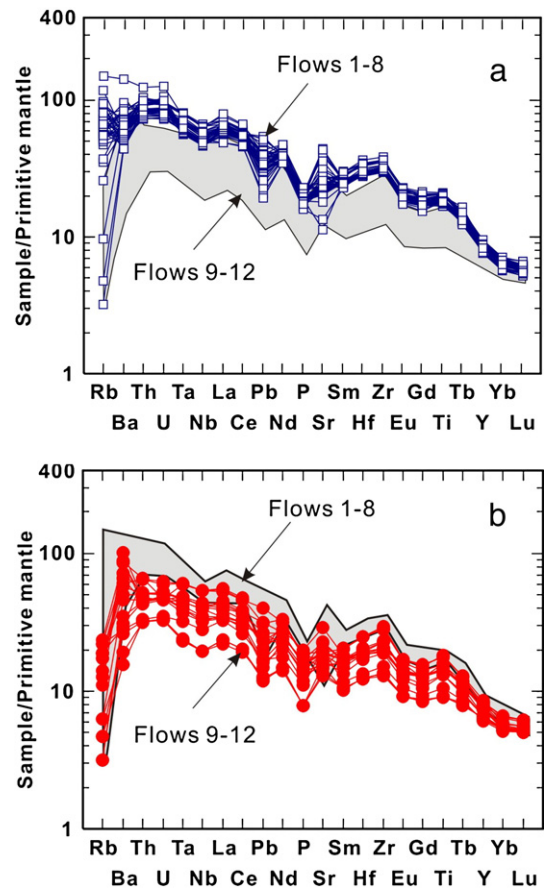


Fig. 8. Primitive mantle-normalized, incompatible trace element patterns for Heishitou basalts. Primitive mantle values are from Sun and McDonough (1989).

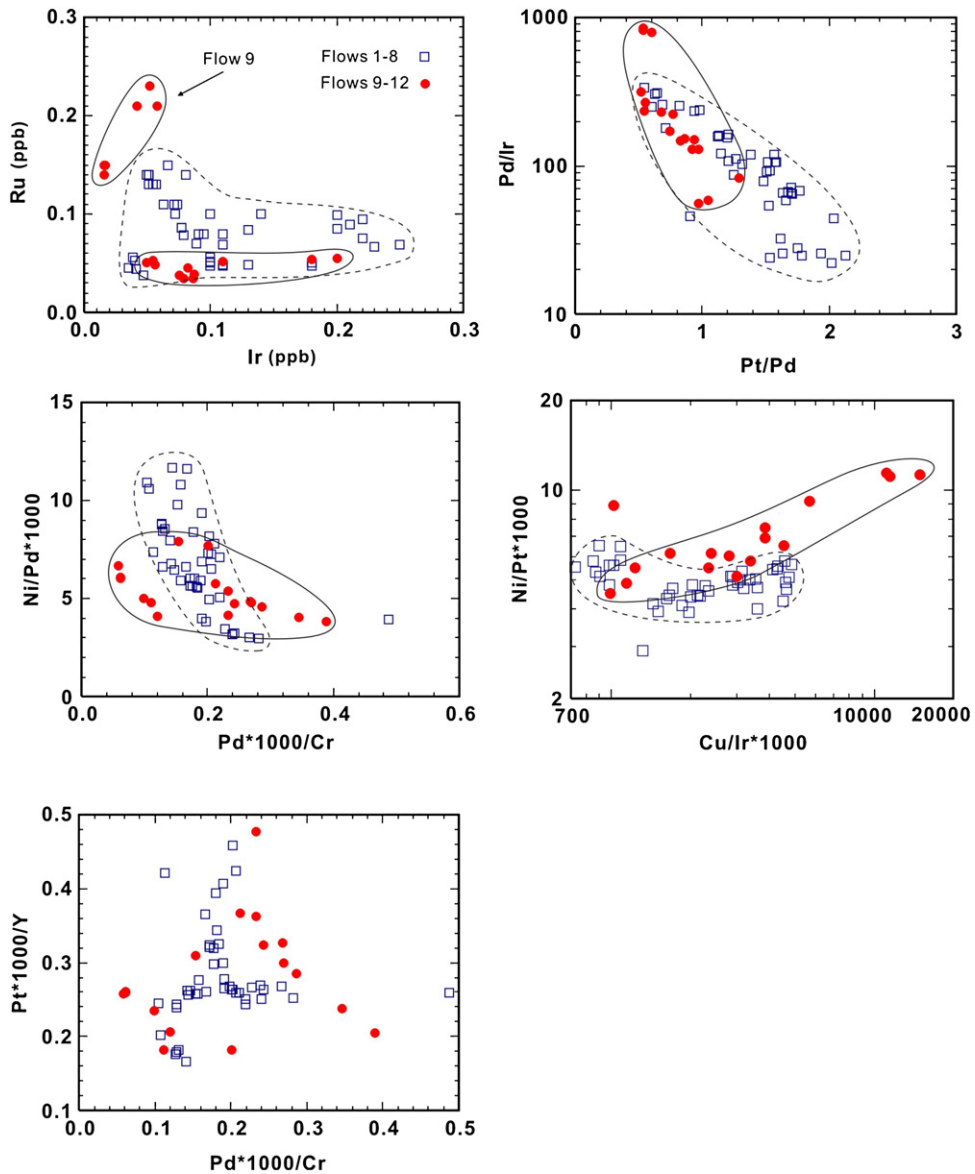


Fig. 9. Plots of Ru vs. Ir, Pd/Ir vs. Pt/Pd, Ni/Pd vs. Pd/Cr and Pd/Y vs. Pd/Cr for the Heishitou basalts.

with lower Pd/Ir ratios (Crocket and Teruta, 1977; Alard et al., 2000). The low Pd/Ir ratios of komatiites and high IPGE of basalts in the Deccan Traps (average Pd/Ir ratio 32) are explained by relatively high degrees of partial melting (Barnes et al., 1985; Zhou, 1994; Crocket and Paul, 2004).

The relatively low Pd/Ir ratios in Flows 1–3 and 5–8 (20–110) compared to Flow 4 (111–339) and Flows 9–12 (56–850) cannot be interpreted as the higher degrees of partial melting, because the concentrations of Pd in these flows are low compared to the other flows. Thus the Pd/Ir ratios are mainly controlled by Pd abundances and the low Pd/Ir ratios cannot represent higher degrees

of partial melting. Fractionation of sulfides and silicates that reduced the Pd and Ir contents in the melts may be the main factor that controlled the Pd/Ir ratios.

All the basaltic samples have MgO contents ranging from 4 to 6 wt.% and Mg# ranging from 34.3 to 48.4 (Supplementary Table 1) suggesting that a considerable amount of fractionation took place prior to the eruption of the lavas. This interpretation is supported by the low Ni and Cr contents and high Cu/Ni ratios of these rocks (Supplementary Table 1, Fig. 5a).

Early crystallization of laurite would also be a very effective means of removing the IPGE from a magma.

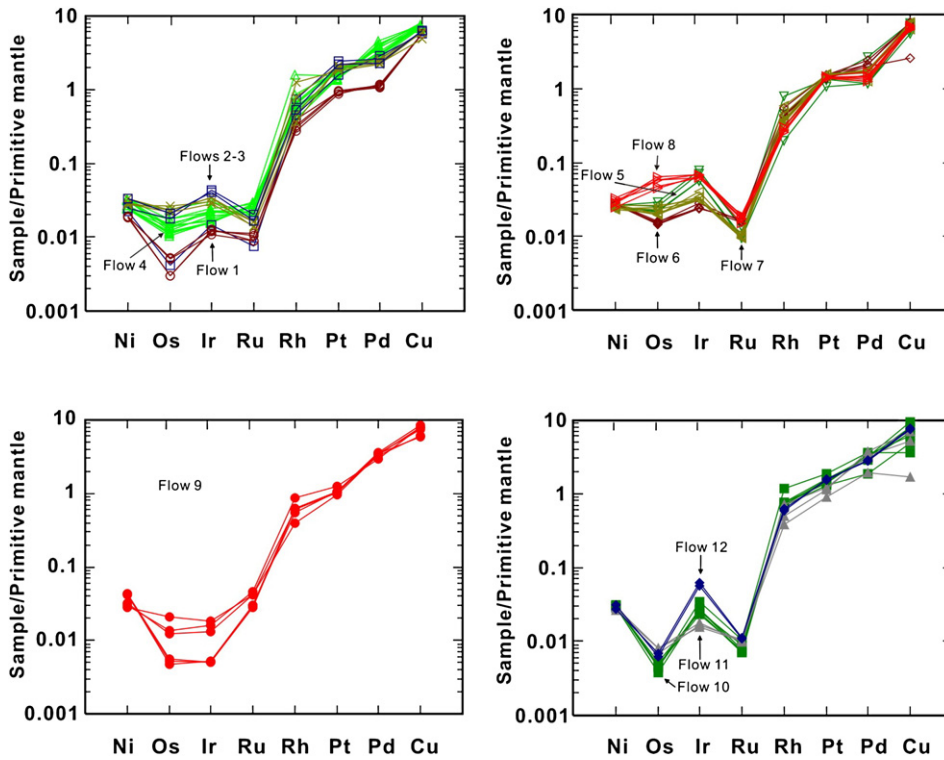


Fig. 10. Primitive mantle-normalized PGE patterns of different flows for the Heishitou basalts. Primitive mantle values are from Sun and McDonough (1989).

During the early stages of crystal fractionation, IPGE may form laurite and Os–Ir–Ru alloys (Capobianco and Drake, 1990; Amosse et al., 1990; Peck and Keays, 1990; Merkle, 1998), and enclosed in early phases, such as chromite and olivine (Stockman, 1984), suggests that these may be physically incorporated as submicroscopic grains in major fractionating phases (Zhou, 1994), effectively removing the IPGE from the melt. In this fashion, precipitation of IPGE-hosting alloys can produce strong fractionation between PPGE and IPGE in the melt. Precipitation of

laurite or Ru–Os–Ir alloy (or both) will cause IPGE depletion and PPGE enrichment in S-undersaturated melts. The steep primitive mantle-normalized PGE patterns of the Heishitou basalts clearly indicate such fractionation

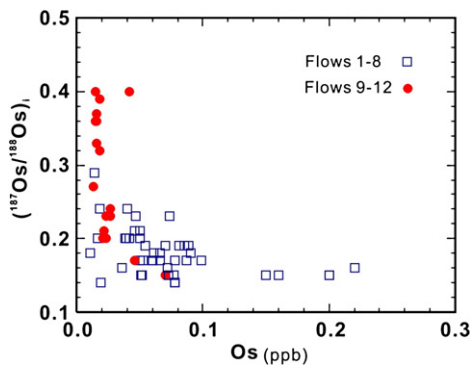


Fig. 11. Plots of initial $^{187}\text{Os}/^{188}\text{Os}_i$ vs. Os contents for the Heishitou basalts.

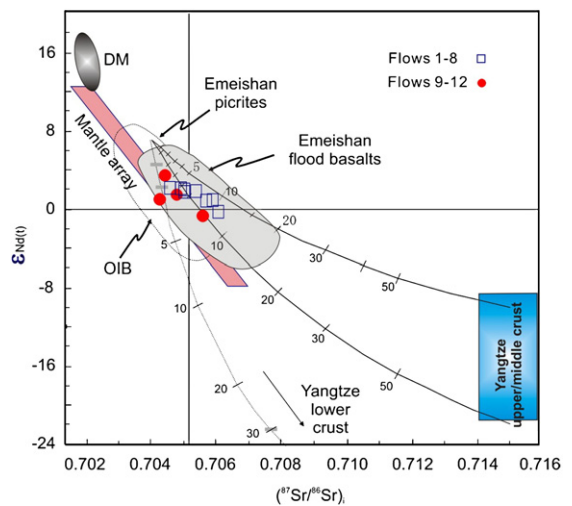


Fig. 12. Plots of $(\text{Nb}/\text{Th})_{\text{PM}}$ vs. $(\text{Th}/\text{Yb})_{\text{PM}}$, showing variations in crustal contamination for the Heishitou basalts. Data source: PM, N-MORB and OIB, Sun and McDonough (1989); Emeishan picrites, Zhang et al. (2004); the upper crust, Taylor and McLennan (1985).

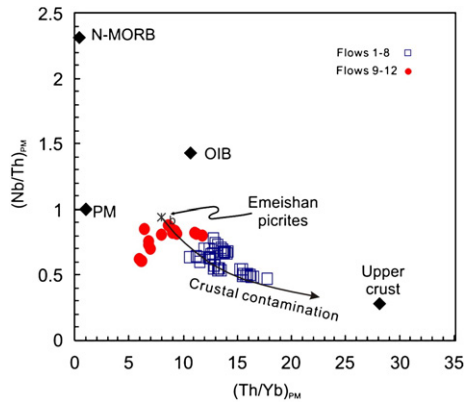


Fig. 13. Variation diagram of $(^{87}\text{Sr}/^{86}\text{Sr})_i$ and $\epsilon_{\text{Nd}(t)}$ ($t=260$ Ma) of different flows for Heishitou basalts. DM (depleted mantle) and mantle array trends are after Zindler and Hart (1986). OIB data are from Wilson (1989). Emeishan flood basalt data are from Xu et al. (2001) and Xiao et al. (2004). The Yangtze upper/middle crust and lower crust data are from Gao et al. (1999), Ma et al. (2000), and Chen and Jahn (1998). The numbers indicate the percentages of participation of the crustal materials. The calculated parameters of Nd (ppm), $\epsilon_{\text{Nd}(t)}$, Sr (ppm) and $(^{87}\text{Sr}/^{86}\text{Sr})_i$ are 4.4, +7, 102 and 0.704 from picrites in northern Vietnam as parental magmas; 20, -22, 220, 0.715 and 20, -10, 220, 0.715 as two components of the Yangtze middle/upper crust.

between IPGE and PPGE (Fig. 10). The relatively high PPGE and low IPGE of these basalts suggest that most of the melts were S-undersaturated and may have undergone early fractionation of chromite or olivine.

6.3.2. Negative Ru anomalies

The crystallization of laurite during the early stages of fractionation may cause a negative Ru anomaly on primitive mantle-normalized chalcophile element patterns. Most Heishitou basalts, except those from Flows 4 and 9, have such negative Ru anomalies (Fig. 10). It has been documented that laurite is stable up to ~ 1275 °C at $\log f_{\text{S}_2}$ of -2.0 and is replaced by a Ru alloy at higher temperatures (Brenan and Andrews, 2001). Therefore, both laurite and Ru–Os–Ir alloys are stable at liquidus temperatures of chromian spinel in mafic magma. Because of its high thermal stability, laurite can be an early primary magmatic phase and can be entrapped in other crystallizing minerals phases, such as chromian spinel (e.g., Hiemstra, 1979; Merkle, 1992; Righter et al., 2004). High Ru concentrations in these minerals relative to Os and Ir can lead to the preferential removal of Ru from silicate magmas and negative Ru anomalies in primitive mantle-normalized PGE diagrams.

The negative Ru anomalies in flood basalts and positive anomalies in ultramafic rocks and chromites were documented elsewhere in the world. Philipp et al. (2001) reported negative Ru anomalies in the basalt of the

seaward-dipping reflector sequence, SE Greenland coast, similar to the Ru anomalies in the Heishitou basalts. Chazey and Neal (2005) reported positive Ir anomalies and negative Ru anomalies in basalts from the Kerguelen Plateau. Osmium and Ru are enriched in mss (mono-sulfide solid solution) inclusions in mantle xenocrysts (Aulbach et al., 2004), and positive Ru anomalies have been reported in chromites from the Troodos complex (Büchl et al., 2004) and ophiolites in China (Zhou et al., 1998). Lorand et al. (2004) reported positive Os and Ru anomalies in dunites and some harzburgites, and Puchtel

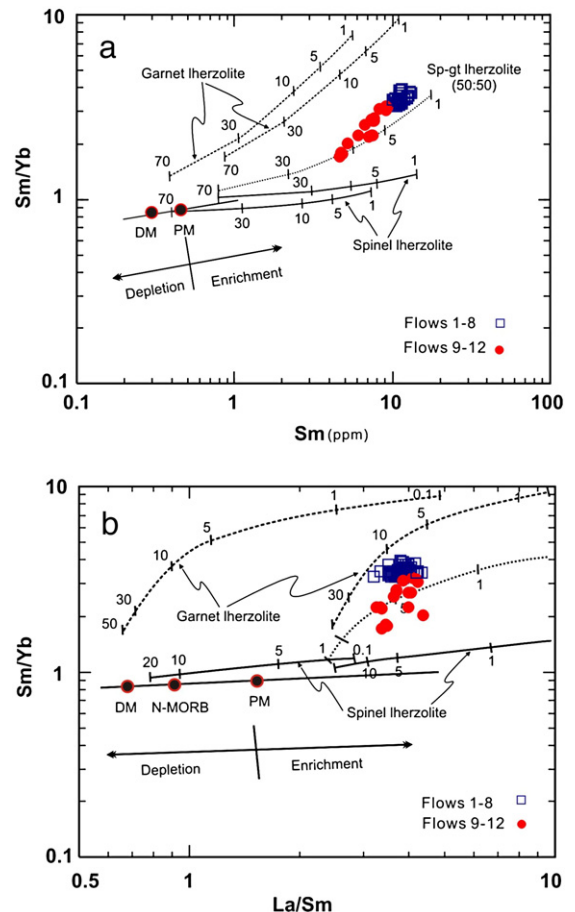


Fig. 14. Plots of Sm/Yb vs. Sm and Sm/Yb vs. La/Sm showing melt curves for Heishitou basalts. Data obtained using the non-modal batch melting equations of Shaw (1970). Melt curves are drawn for spinel–lherzolite (with mode and melt mode of $\text{Ol}_{0.530} + \text{Opx}_{0.270} + \text{Cpx}_{0.170} + \text{Sp}_{0.030}$ and $\text{Ol}_{0.060} + \text{Opx}_{0.280} + \text{Cpx}_{0.670} + \text{Sp}_{0.110}$, respectively, Kinzler, 1997) and for garnet–lherzolite (with mode and melt mode of $\text{Ol}_{0.600} + \text{Opx}_{0.200} + \text{Cpx}_{0.100} + \text{Gt}_{0.100}$ and $\text{Ol}_{0.030} + \text{Opx}_{0.160} + \text{Cpx}_{0.880} + \text{Gt}_{0.090}$, respectively, Walter, 1998). Mineral/matrix partition coefficients and DMM are from the compilation of McKenzie and O’Nions (1991, 1995); PM and N-MORB compositions are from Sun and McDonough (1989).

and Humayun (2001) observed positive Ru anomalies in olivine, chromite and sulfide. Handler and Bennett (1999) reported relatively high Ru abundances of some peridotites and abyssal peridotites and suggested that the Ru abundances in the mantle may be higher than predicted by chondritic abundances and may be regionally heterogeneous. Fiorentini et al. (2004) reported a strong positive relationship between Cr and Ru in Agnew komatiite, and suggested that Ru is soluble in chromite during crystallization, causing Ru positive anomalies. Positive Ru anomalies in olivine and chromite and negative anomalies in basalts may reflect removal of laurite in the primary magma, followed by coprecipitation with chromian spinel, olivine or sulfide fractionation.

Based on the above discussion, we interpret the negative Ru anomalies of most of the Heishitou basalts (Fig. 10) to indicate fractionation of laurite or Os–Ir–Ru alloys in the primary magma. Flows 4 and 9, the only ones without negative Ru anomalies, have relatively high Cr and Ru (Tables 1 and 3, Fig. 5b), suggesting relatively primitive nature of the magma.

6.3.3. Pt and Pd fractionation

As described by Lightfoot and Keays (2005), there are three ways for changing the Pt/Pd ratios in the melting: (1) fractionation of a S-saturated melt may change the Pt/Pd ratio, because the Pd is more chalcophile than Pt (Vogel and Keays, 1997), (2) fractionation of a S-undersaturated magma with segregation of silicates and possibly spinels, and (3) accumulation of a phase which does not host either Pd or Pt. The primitive mantle has a Pt/Pd ratio of about 1.82 (McDonough and Sun, 1995). The lower ratios of Heishitou can be interpreted as the result of early fractionation of silicate minerals, chromite and possibly platinum-group minerals from S-undersaturated melts. Because Pt has a larger partition coefficient than Pd between silicate magma and olivine phenocrysts (Momme et al., 2002) or between the fractionating assemblage (OI±PGE-phases) and komatiitic melt (Puchtel and Humayun, 2000, 2001), Pt will be preferentially removed from a sulfide-undersaturated magma undergoing silicate mineral fractionation (Momme et al., 2002). Thus, the fractionation of Pt and Pd in these rocks may reflect olivine fractionation in S-undersaturated melts.

In the East Greenland rifted margin, low-Ti and high-Ti basalts have Pt/Pd ratios ranging from 0.11 to 1.3 and 0.2 to 1.1, respectively, and low Pt/Pd ratios indicate that Pd is much more incompatible than Pt during S-undersaturated differentiation (Momme et al., 2002). Crocket and Paul (2004) reported variable Pd/Ir ratios in the Deccan Traps and suggested that the observed variations resulted mainly from fractional crystallization

of a primitive basaltic melt. They further suggest that crystal fractionation would lead to fractionation of Pt and Pd, resulting in lower Pt/Pd ratios.

Flows 1–3 and 5–8 have the highest Pt/Pd ratios (0.9–2.12), while Flows 4 and 9 have the lowest Pt/Pd ratios (0.54–1.26) and Flows 10–12 have moderate Pt/Pd ratios (0.55–1.29) (Supplementary Table 2, Fig. 5b), suggesting Flows 4 and 9 have relatively extensive silicate fractionation, consistent with the results of Pd/Ir ratios. The strongly negative correlation of Pd/Ir and Pt/Pd ratios in the Heishitou basalts (Fig. 9) indicates that the Pt/Pd ratios may be related to fractionation of non-sulfide phases.

6.4. Sulfur saturation and sulfide segregation

Partial melting of the primitive mantle may lead to the formation of either S-saturated or S-undersaturated magmas. If the melts were S-saturated, the immiscible sulfide liquids would have stayed in the residual mantle, resulting in a PGE-poor magma. If the magma was S-undersaturated, the PGE would have remained in the primary melt, leading to enrichment of PGE, especially PPGE (Seitz and Keays, 1997). At least 25% of partial melting is required to consume all sulfides in the mantle (Keays, 1995; Rehkämper et al., 1999; Momme et al., 2003). Experimental and petrological studies indicate that MORB is S-saturated (Naldrett et al., 1978; Keays, 1995).

The partition coefficients between immiscible sulfide liquid and silicate magma for elements such as Ir and Pd (about 3×10^4) are much higher than those for Ni and Cu (4×10^2 and 10^3 , respectively) (e.g. Barnes and Maier, 1999). Hence, Cu/Pd ratios are useful indicators of the degree of S-saturation of magmas. In immiscible sulfide liquids, Pd and Ir show similar compatible behaviors, whereas Pd is more compatible than Cu (e.g. Fleet et al., 1991; Peach et al., 1994), resulting in relatively constant Pd/Ir ratios, higher and variable Cu/Pd ratios, and lower Cu/Zr ratios in the silicate magma. In contrast, Pd is incompatible and Ir is compatible in olivine or chromite during S-undersaturated differentiation, leading to an increase in Pd/Ir ratios and relatively constant Cu/Pd ratios.

Samples from Heishitou have highly variable Cu/Pd ratios (from 6700 to 45,000) (Supplementary Table 2, Fig. 5b). Flow 1 has relatively high Cu/Pd ratios (38,000–40,000) with low Pt (~6.5 ppb), Pd (~4.3 ppb) contents (Supplementary Table 2) and relatively low Cu/Zr ratios, suggesting sulfide fractionation before emplacement.

Flows 2 and 3 have higher PGE contents and lower Cu/Pd ratios (~18,000), and slightly variable Cu/Zr (0.4–

0.54) and Pd/Ir ratios (70–110), indicating these two flows are from evolved magmas with weak silicate fractionation. Pd/Ir ratios of Flows 4 and 9 are higher than those of other flows, indicating relatively high degree of silicate fractionation. The higher Cu/Zr ratios, lower Cu/Pd ratios, lower Os, Ir and Pt contents, and higher Ru and Pd contents (Fig. 5b), suggesting no S-saturated fractionation for these two flows.

Most samples from Flows 5–8 have relatively constant Os, Ir, Ru, Rh and Pt, but lower Pd contents (Fig. 5b) suggesting a S-saturated trend. Because Pd is more chalcophile than Pt and therefore will be preferentially removed from a sulfide-saturated magma (Vogel and Keays, 1997). The Pd/Ir ratios of these flows are lower than 100, indicating relatively low degree of silicate fractionation before emplacement of these flows.

Samples of Flows 10–12 have low and variable Cu/Pd ratios (6700–22,000) and high and variable Cu/Zr ratios (0.16–1.0) indicating no S-saturated differentiation. They have higher Pd/Ir ratios, lower IPGE and higher Pt and Pd contents than Flows 5–8, indicating a general silicate fractionation trend. As suggested by Bennett et al. (2000), PGE variations of Hawaiian picrites reflect variable amounts of residual sulfide in the mantle source. The variable Cu/Pd and Cu/Zr ratios of Flows 10–12 reflect the complex evolution of the later stages of magma in Heishitou.

7. Conclusions

The Heishitou volcanic sequence includes 12 high-Ti basaltic lava flows with the lower part of the section experienced stronger degree of crustal contamination relative to the upper part. The Heishitou basalts were derived from a garnet–lherzolite, OIB-type mantle source and were produced by about 20% partial melting.

The Os-poor basalts have variable Os isotopic ratios, whereas basalts with higher Os concentrations have relatively constant and less radiogenic values. Only minor amounts of crustal contamination are required to alter the Os isotopic composition of Os-poor basaltic magma.

The relatively high PPGE and low IPGE concentrations of these basalts suggest derivation from a magma that has not experienced S-saturation. Crystal fractionation played an important role in the fractionation between PPGE and IPGE and between Pt and Pd. The negative Ru anomalies on primitive mantle-normalized PGE patterns of the Heishitou basalts result from fractionation of laurite or Os–Ir–Ru alloys in the primary magma.

Acknowledgements

This study was supported by the National Natural Science Foundation of China (40573049) and a grant from the Research Grants Council of Hong Kong (HKU7057/05P). We thank Dr. Zhang Zhengwei for the help with field work in Guizhou Province (SW China), Mr. Kwan Nang Pang, Ms. Christina Y. Wang, and Mr. Junhong Zhao for reading an early draft of this paper, and Ms. Xiao Fu for the help with the XRF analyses. Two reviewers provide thorough reviews that resulted in significant improvement of this paper.

Appendix A. Supplementary data

Supplementary data associated with this article can be found, in the online version, at [doi:10.1016/j.chemgeo.2007.11.004](https://doi.org/10.1016/j.chemgeo.2007.11.004).

References

- Alard, O., Griffin, W.L., Lorand, J.P., 2000. Non-chondritic distribution of the highly siderophile elements in mantle sulphides. *Nature* 407, 891–894.
- Aldanmaz, E., Pearce, J.A., Thirlwall, M.F., Mitchell, J.G., 2000. Petrogenetic evolution of late Cenozoic, post-collision volcanism in western Anatolia, Turkey. *J. Volcanol. Geotherm. Res.* 102, 67–95.
- Ali, J.R., Lo, C.H., Thompson, G.M., Song, X., 2004. Emeishan Basalt Ar–Ar overprint ages define several tectonic events that affected the western Yangtze Platform in the Mesozoic and Cenozoic. *J. Asian Earth Sci.* 23, 163–178.
- Amosse, J., Allibert, M., Fischer, W., Piboule, M., 1990. Experimental study of the solubility of platinum and iridium in basic silicate melts—implications for the differentiation of platinum-group elements during magmatic processes. *Chem. Geol.* 81, 45–53.
- Arndt, N.T., Czamanske, G.K., Wooden, J.L., Fedorenko, V.A., 1993. Mantle and crustal contributions to continental flood volcanism. *Tectonophysics (Amst.)* 223, 39–52.
- Arndt, N.T., Chauvel, C., Czamanske, G.K., Fedorenko, V.A., 1998. Two mantle sources, two plumbing systems: tholeiitic and alkaline magmatism of the Maymecha River basin, Siberian flood volcanic province. *Contrib. Mineral. Petrol.* 133, 297–313.
- Arndt, N.T., Czamanske, G.K., Walker, R.J., Chauvel, C., Fedorenko, V.A., 2003. Geochemistry and origin of the intrusive hosts of the Noril'sk–Talnakh Cu–Ni–PGE sulfide deposits. *Econ. Geol.* 8, 495–515.
- Aulbach, S., Griffin, W.L., Pearson, N.J., O'Reilly, S.Y., Kivi, K., Doyle, B.J., 2004. Mantle formation and evolution, Slave Craton: constraints from HSE abundances and Re–Os isotope systematics of sulfide inclusions in mantle xenocrysts. *Chem. Geol.* 208, 61–88.
- Barnes, S.J., Maier, W.D., 1999. The fractionation of Ni, Cu, and the noble metals in silicate and sulphide liquids. In: Keays, R.R., Leshner, C.M., Lightfoot, P.C., Farrow, C.E.G. (Eds.), *Dynamic Processes in Magmatic Ore Deposits and Their Application to Mineral Exploration*. Geological Association of Canada, Short course notes, vol. 13, pp. 69–106.

- Barnes, S.J., Naldrett, A.J., Gorton, M.P., 1985. The origin of the fractionation of platinum-group elements in terrestrial magmas. *Chem. Geol.* 53, 303–323.
- Bennett, V.C., Norman, M.D., Garcia, M.O., 2000. Rhenium and platinum group element abundances correlated with mantle source components in Hawaiian picrites: sulphides in the plume. *Earth Planet. Sci. Lett.* 183, 513–526.
- Bezmen, N.I., Asif, M., Brüggmann, G.E., Romanenko, I.M., Naldrett, A.J., 1994. Distribution of Pd, Rh, Ru, Ir, Os and Au between sulfide and silicate metals. *Geochim. Cosmochim. Acta* 58, 1251–1260.
- Brenan, J.M., Andrews, D., 2001. High-temperature stability of laurite and Ru–Os–Ir alloy and their role in PGE fractionation in mafic magmas. *Can. Mineral.* 39, 341–360.
- Brüggmann, G.E., Naldrett, A.J., Asif, M., Lightfoot, P.C., Gorbachev, N.S., Fedorenko, V.A., 1993. Siderophile and chalcophile metals as tracers of the evolution of the Siberian Trap in the Noril'sk region, Russia. *Geochim. Cosmochim. Acta* 57, 2001–2018.
- Büchl, A., Brüggmann, G., Batanova, V.G., 2004. Formation of podiform chromitite deposits: implications from PGE abundances and Os isotopic compositions of chromites from the Troodos complex, Cyprus. *Chem. Geol.* 208, 217–232.
- Capobianco, C.J., Drake, M.J., 1990. Partitioning of ruthenium, rhodium, and palladium between spinel and silicate melt and implications for platinum group element fractionation trends. *Geochim. Cosmochim. Acta* 54, 869–874.
- Chazey III, W.J., Neal, C.R., 2005. Platinum-group element constraints on source composition and magma evolution of the Kerguelen Plateau using basalts from ODP Leg 183. *Geochim. Cosmochim. Acta* 69, 4685–4701.
- Chen, J.F., Jahn, B.M., 1998. Crustal evolution of southeastern China: Nd and Sr isotopic evidence. *Tectonophysics* 284, 101–133.
- Chen, F.K., Siebel, W., Satir, M., Terzioğlu, M.N., Saka, K., 2002. Geochronology of the Karadere basement (NW Turkey) and implications for the geological evolution of the Istanbul zone. *Int. J. Earth Sci.* 91, 469–481.
- Chen, F.K., Li, X.H., Wang, X.L., Li, Q.L., Siebel, W., 2007. Zircon age and Nd–Hf isotopic composition of the Yunnan Tethyan belt, southwestern China. *Int. J. Earth Sci.* 96, 1179–1194.
- Chung, S.L., Jahn, B.M., 1995. Plume–lithosphere interaction in generation of the Emeishan flood basalts at the Permian–Triassic boundary. *Geology* 23, 889–892.
- Crocket, J.H., 2000. PGE in fresh basalt, hydrothermal alteration products, and volcanic incrustations of Kilauea volcano, Hawaii. *Geochim. Cosmochim. Acta* 64, 1791–1807.
- Crocket, J.H., Teruta, Y., 1977. Palladium, iridium and gold contents of mafic and ultramafic rocks drilled from the mid-Atlantic ridge, Leg 37, Deep Sea Drilling Project. *Can. J. Earth Sci.* 14, 777–784.
- Crocket, J.H., Paul, D.K., 2004. Platinum-group elements in Deccan mafic rocks: a comparison of suites differentiated by Ir content. *Chem. Geol.* 208, 273–291.
- Edwards, C.M.H., Menzies, M.A., Thirlwall, M.F., Morris, J.D., Leeman, W.P., Harmon, R.S., 1994. The transition to potassic alkaline volcanism in island arcs: the Ringgit–Beser complex, east Java, Indonesia. *J. Petrol.* 35, 1557–1595.
- Ely, J.C., Neal, C.R., 2003. Using platinum-group elements to investigate the origin of the Ontong Java Plateau, SW Pacific. *Chem. Geol.* 196, 235–257.
- Esser, B.K., Turekian, K.K., 1993. The osmium isotopic composition of the continental crust. *Geochim. Cosmochim. Acta* 57, 3093–3104.
- Fiorentini, M.L., Stone, W.E., Beresford, S.W., Barley, M.E., 2004. Platinum-group element alloy inclusions in chromites from Archaean mafic–ultramafic units: evidence from the Abitibi and the Agnew–Wiluna Greenstone Belts. *Mineral. Petrol.* 82, 341–355.
- Fleet, M.E., Tronnes, R.G., Stone, W.E., 1991. Partitioning of platinum group elements in the Fe–O–S system to 11 GPa and their fractionation in the mantle and meteorites. *J. Geophys. Res.* 96, 21949–21958.
- Gao, S., Ling, W.L., Qiu, Y.M., Lian, Z., Hartmann, G., Simon, K., 1999. Contrasting geochemical and Sm–Nd isotopic compositions of Archean metasediments from the Kongling high-grade terrain of the Yangtze craton: evidence for cratonic evolution and redistribution of REE during crustal anatexis. *Geochim. Cosmochim. Acta* 63, 2071–2088.
- Green, N.L., 2006. Influence of slab thermal structure on basalt source regions and melting conditions: REE and HFSE constraints from the Garibaldi volcanic belt, northern Cascadia subduction system. *Lithos* 87, 23–49.
- Gros, M., Lorand, J.P., Luguët, A., 2002. Analysis of platinum group elements and gold in geological materials using NiS fire assay and Te coprecipitation; the NiS dissolution step revisited. *Chem. Geol.* 185, 179–190.
- Gurenko, A.A., Chaussidon, M., 1995. Enriched and depleted primitive melts included in olivine from Icelandic tholeiites: origin by continuous melting of a single mantle column. *Geochim. Cosmochim. Acta* 59, 2905–2917.
- Handler, M.R., Bennett, V.C., 1999. Behavior of platinum-group elements in the subcontinental mantle of eastern Australia during variable metasomatism and melt depletion. *Geochim. Cosmochim. Acta* 63, 3597–3618.
- Hanski, E., Walker, R.J., Huhma, H., Polyakov, G.V., Balykin, P.A., Hoa, T.T., Phuong, N.T., 2004. Origin of the Permian–Triassic komatiites, northwestern Vietnam. *Contrib. Mineral. Petrol.* 147, 453–469.
- He, B., Xu, Y.G., Chung, S.L., Xiao, L., Wang, Y.M., 2003. Sedimentary evidence for a rapid, kilometer scale crustal doming prior to the eruption of the Emeishan flood basalts. *Earth Planet. Sci. Lett.* 213, 391–405.
- Hiemstra, S.A., 1979. The role of collectors in the formation of the platinum deposits in the Bushveld Complex. *Can. Mineral.* 17, 469–482.
- IUPAC (International union of pure applied chemistry), 1991. Isotopic compositions of the elements 1989. *Pure Appl. Chem.* 63, 991–1002.
- Johnson, K.T.M., 1998. Experimental determination of partition coefficients for rare earth and high-field-strength elements between clinopyroxene, garnet, and basaltic melt at high pressures. *Contrib. Mineral. Petrol.* 133, 60–68.
- Keays, R.R., 1995. The role of komatiitic magmatism and S-saturation in the formation of ore deposits. *Lithos* 34, 1–18.
- Kinzler, R.J., 1997. Melting of mantle peridotite at pressures approaching the spinel to garnet transition: application to mid-ocean ridge basalt petrogenesis. *J. Geophys. Res.* 102, 853–874.
- Koide, M., Goldberg, E.D., Niemeyer, S., Gerlach, D., Hodge, V., Bertine, K., Padova, A., 1991. Osmium in marine sediments. *Geochim. Cosmochim. Acta* 55, 1641–1648.
- Liang, Q., Jing, H., Gregoire, D.C., 2000. Determination of trace elements in granites by inductively coupled plasma mass spectrometry. *Talanta* 51, 507–513.
- Lightfoot, P.C., Keays, R.R., 2005. Siderophile and chalcophile metal variations in flood basalts from the Siberian Trap, Noril'sk Region: implications for the Origin of the Ni–Cu–PGE Sulfide Ores. *Econ. Geol.* 100, 439–462.
- Lorand, J.P., Delpech, G., Grégoire, M., Moine, B., O'Reilly, S.Y., Cottin, J.Y., 2004. Platinum-group elements and the multistage metasomatic

- history of Kerguelen lithospheric mantle (South Indian Ocean). *Chem. Geol.* 208, 195–215.
- Ma, C.Q., Ehlers, C., Xu, C.H., Li, Z.C., Yang, K.G., 2000. The roots of the Dabieshan ultrahigh-pressure metamorphic terrane: constraints from geochemistry and Nd–Sr isotope systematics. *Precambrian Res.* 102, 279–301.
- Maier, W.D., Barnes, S.-J., 1999. Platinum-group element in silicate rocks of the lower, critical and main zones at union section, western Bushveld complex. *J. Petrol.* 40, 1647–1671.
- Maier, W.D., Barnes, S.-J., Marsh, J.S., 2003. The concentrations of the noble metals in Southern African flood-type basalts and MORB: implications for petrogenesis and magmatic sulphide exploration. *Contrib. Mineral. Petrol.* 146, 44–61.
- McDonough, W.F., Sun, S.-S., 1995. The composition of the earth. *Chem. Geol.* 120, 223–253.
- McKenzie, D.P., O’Nions, R.K., 1991. Partial melt distribution from inversion of rare earth element concentrations. *J. Petrol.* 32, 1021–1091.
- McKenzie, D.P., O’Nions, R.K., 1995. The source regions of ocean island basalts. *J. Petrol.* 36, 133–159.
- Meisel, T., Moser, J., 2004. Reference materials for geochemical PGE analysis: new analytical data for Ru, Rh, Pd, Os, Ir, Pt and Re by isotope dilution ICP-MS in 11 geological reference materials. *Chem. Geol.* 208, 319–338.
- Meisel, T., Walker, R.J., Morgan, J.W., 1996. The osmium isotopic composition of the primitive upper mantle. *Nature* 383, 517–520.
- Merkle, R.K.W., 1992. Platinum-group minerals in the middle group of chromitite layers at Marikana, western Bushveld Complex: indications for collection mechanisms and postmagmatic modification. *Can. J. Earth Sci.* 29, 209–221.
- Merkle, R.K.W., 1998. Proportions of magmatic platinum-group minerals and evolution of mineralizing processes, UG-1 chromitite layer, Bushveld Complex. In: Laverov, N.P., Distler, V.V. (Eds.), *International Platinum*. Theophrastos Publications, Theophrastus, pp. 43–53.
- Momme, P., Brooks, C.K., Tegner, C., Keays, R.R., 2002. The behavior of platinum-group elements in basalts from East Greenland rifted margin. *Contrib. Mineral. Petrol.* 143, 133–153.
- Momme, P., Oskarsson, N., Keays, R.R., 2003. Platinum-group elements in the Icelandic rift system: melting processes and mantle sources beneath Iceland. *Chem. Geol.* 196, 209–234.
- Naldrett, A.J., Goodwin, A.M., Fisher, T.L., Ridler, R.H., 1978. Sulfur-content of Archean volcanic-rocks and a comparison with ocean-floor basalts. *Can. J. Earth Sci.* 15, 715–728.
- Palmer, M.R., Turekian, K.K., 1986. $^{187}\text{Os}/^{186}\text{Os}$ in marine manganese nodules and the constraints on the crustal geochemistries of rhenium and osmium. *Nature* 319, 216–220.
- Palmer, M.R., Falkner, K.K., Turekian, K.K., Calvert, S.E., 1988. Sources of osmium isotopes in manganese nodules. *Geochim. Cosmochim. Acta* 52, 1197–1202.
- Peach, C.L., Mathez, E.A., Keays, R.R., Reeves, S.J., 1994. Experimentally determined sulfide melt–silicate melt partition coefficients for iridium and palladium. *Chem. Geol.* 117, 361–377.
- Pearce, J.A., Lippard, S.J., Roberts, S., 1984. Characteristics and tectonic significance of suprasubduction zone ophiolites. In: Kokelaar, B.P., Howells, M.F. (Eds.), *Marginal Basin Geology*. *Geol. Soc. Special Publ.*, vol. 16, pp. 77–94.
- Peck, D.C., Keays, R.R., 1990. Geology, geochemistry, and origin of platinum-group element-chromitite occurrences in the Heazlewood River Complex, Tasmania. *Econ. Geol.* 85, 765–793.
- Philipp, H., Eckhardt, J.-D., Puchelt, H., 2001. Platinum-group element in basalts of the seaward-dipping reflector sequence, SE Greenland coast. *J. Petrol.* 42, 407–432.
- Potts, P.J., Kane, J.S., 2005. International association of geoanalysts certificate of analysis: certified reference material OU-6 (Penrhyn slate). *Geostand. Geoanal. Res.* 29, 233–236.
- Puchtel, I., Humayun, M., 2000. Platinum group elements in Kostomuksha komatiites and basalts: implications for oceanic crust recycling and core–mantle interaction. *Geochim. Cosmochim. Acta* 64, 4227–4242.
- Puchtel, I.S., Humayun, M., 2001. Platinum group element fractionation in a komatiitic basalt lava lake. *Geochim. Cosmochim. Acta* 65, 2979–2993.
- Qi, L., Zhou, M.-F., Wang, C.Y., 2004. Determination of low concentrations of platinum group elements in geological samples by ID-ICP-MS. *J. Anal. At. Spectrom.* 19, 1335–1339.
- Qi, L., Zhou, M.-F., Wang, C.Y., Sun, M., 2007. Evaluation of the determination of Re and PGEs abundance of geological samples by ICP-MS coupled with a modified Carius tube digestion at different temperatures. *Geochem. J.* 41, 407–414.
- Rehkämper, M., Halliday, A.N., Fitton, J.G., Lee, D.-C., Wieneke, M., Arndt, N.T., 1999. Ir, Ru, Pt and Pd in basalts and komatiites: new constraints for the geochemical behavior of the platinum-group elements in the mantle. *Geochim. Cosmochim. Acta* 63, 3915–3934.
- Reisberg, L., Zindler, A., Marcantonio, F., White, W., Wyman, D., Weaver, B., 1993. Os isotope systematics in ocean island basalts. *Earth Planet. Sci. Lett.* 120, 149–167.
- Righter, K., Campbell, A.J., Humayun, M., Hervig, R.L., 2004. Partitioning of Ru, Rh, Pd, Re, Ir, and Au between Cr-bearing spinel, olivine, pyroxene and silicate melts. *Geochim. Cosmochim. Acta* 68, 867–880.
- Roddick, J.C., Sullivan, R.W., Dudás, F.Ö., 1992. Precise calibration of Nd tracer isotopic composition for Sm–Nd studies. *Chem. Geol.* 97, 1–8.
- Schoenberg, R., Nögler, T.F., Kramers, J.D., 2000. Precise Os isotope ratio and Re–Os isotope dilution measurements down to the picogram level using multicollector inductively coupled plasma mass spectrometry. *Int. J. Mass Spectrom.* 197, 85–94.
- Seitz, H.M., Keays, R.R., 1997. Platinum group element segregation and mineralization in a noritic ring complex formed in Proterozoic siliceous high magnesium basalt magmas in the Vestfold Hill, Antarctica. *J. Petrol.* 38, 703–725.
- Shaw, D.M., 1970. Trace element fractionation during anatexis. *Geochim. Cosmochim. Acta* 34, 237–243.
- Shirey, S.B., Walker, R.J., 1995. Carius tube digestion for low-blank rhenium–osmium analysis. *Anal. Chem.* 67, 2136–2141.
- Song, X.Y., Zhou, M.F., Hou, Z.Q., Cao, Z.M., Wang, Y.L., Li, Y.G., 2001. Geochemical constraints on the mantle source of the upper Permian Emeishan continental flood basalts, southwestern China. *Int. Geol. Rev.* 43, 213–225.
- Song, X.Y., Zhou, M.F., Cao, Z.-M., Robinson, P.T., 2004. Late Permian rifting of the South China Craton caused by the Emeishan mantle plume? *J. Geol. Soc. (Lond.)* 161, 773–781.
- Song, X.Y., Zhou, M.F., Keays, R.R., Cao, Z., Sun, M., Qi, L., 2006. Geochemistry of the Emeishan flood basalts at Yangliuping, Sichuan, SW China: implications for sulfide segregation. *Contrib. Mineral. Petrol.* 152, 53–74.
- Stockman, H.W., 1984. Electron-microprobe characterization of minute platinum-group mineral inclusion-limits on accuracy. *Scanning Electron Microsc. (Part 3)*, 1097–1109.
- Sun, S.S., McDonough, W.F., 1989. Chemical and isotopic systematics of oceanic basalts: implications for mantle composition and processes. In: Saunders, A.D., Norry, M.J. (Eds.), *Magmatism in the Ocean Basins*. Geological Society Special Publication, vol. 42, pp. 313–345.

- Taylor, S.R., McLennan, S.M., 1985. The continental crust: its composition and evolution. An Examination of the Geochemical Record Preserved in Sedimentary Rocks. Blackwell Scientific Publication, Oxford. 46 pp.
- Thompson, M., Potts, P.J., Kane, J.S., Wilson, S., 2000. GeoPT5. An international proficiency test for analytical geochemistry laboratories—report on round 5 (August 1999). *Geostand. Geoanal. Res.* 24, E1–E28.
- Vogel, D.C., Keays, R.R., 1997. The petrogenesis and platinum-group element geochemistry of the Newer Volcanic Province, Victoria, Australia. *Chem. Geol.* 136, 181–204.
- Widom, E., Shirey, S.B., 1996. Os isotope systematics in the Azores: implications for mantle plume sources. *Earth Planet. Sci. Lett.* 142, 451–466.
- Widom, E., Hoernle, K.A., Shirey, S.B., Schmincke, H.-U., 1999. Os isotope systematics in the canary islands and madeira: lithospheric contamination and mantle plume signatures. *J. Petrol.* 40, 279–296.
- Wilson, M., 1989. *Igneous Petrogenesis*. Unwin Hyman, London, pp. 245–285.
- Wooden, J.L., Czamanske, G.K., Fedorenko, V.A., Arndt, N.T., Chauvel, C., Bouse, R.M., King, B.W., Knight, R.J., Siems, D.F., 1993. Isotopic and trace-element constraints on mantle and crustal contributions to Siberian continental flood basalts, Noril'sk area, Siberia. *Geochim. Cosmochim. Acta* 57, 3677–3704.
- Xiao, L., Xu, Y.G., Chung, S.L., He, B., Mei, H.J., 2003. Chemostratigraphic correlation of upper Permian lavas, from Yunnan Province, China: extent of the Emeishan large igneous province. *Int. Geol. Rev.* 45, 754–766.
- Xiao, L., Xu, Y.G., Mei, H.J., Zhang, Y.F., He, B., Pirajno, F., 2004. Distinct mantle sources of low-Ti and high-Ti basalts from the western Emeishan large igneous province, SW China: implications for plume–lithosphere interaction. *Earth Planet. Sci. Lett.* 228, 525–546.
- Xu, Y.G., Chung, S.L., Jahn, B.M., Wu, G.Y., 2001. Petrologic and geochemical constraints on the petrogenesis of Permian–Triassic Emeishan flood basalts in southwestern China. *Lithos* 58, 145–168.
- Xu, Y.G., He, B., Chung, S.L., Menzies, M.A., Frey, F.A., 2004a. The geologic, geochemical and geophysical consequences of plume involvement in the Emeishan flood basalt province. *Geology* 30, 917–920.
- Xu, Y.G., Chung, S.L., Ma, J.L., Shi, L.B., 2004b. Contrasting Cenozoic lithospheric evolution and architecture in the western and eastern Sino-Korean craton: constraints from geochemistry of basalts and mantle xenoliths. *J. Geol.* 112, 593–605.
- Yan, D.P., Zhou, M.F., Song, F., Fu, Z., 2003a. Structural style and tectonic significance of the Jianglang Metamorphic Core complex in the Eastern Margin of the Tibetan Plateau, China. *J. Struct. Geol.* 25, 239–254.
- Yan, D.P., Zhou, M.F., Song, H.L., Wang, X.W., Malpas, J., 2003b. Origin and tectonic significance of a Mesozoic multi-layer overthrust within the Yangtze Block (South China). *Tectonophysics* 361, 239–254.
- Zhang, Y.X., Luo, Y.N., Yang, Z.X., 1988. Panxi Rift. Geological Publishing House, Beijing. 466 pp. (in Chinese with English abstract).
- Zhang, H.F., Sun, M., Lu, F.X., Zhou, X.H., Zhou, M.F., Liu, Y.S., Zhang, G.H., 2001. Moderately depleted lithospheric mantle underneath the Yangtze Block: evidence from a garnet lherzolite xenolith in the Dahongshan kimberlite. *Geochem. J.* 35, 315–331.
- Zhang, Z.C., Wang, F.S., Hao, Y.L., Mahoney, J.J., 2004. Geochemistry of the picrites and associated basalts from the Emeishan large igneous basalt province and constrains on their source region. *Acta Geol. Sin.* 78, 171–180 (in Chinese with English abstract).
- Zhong, H., Zhou, X.H., Zhou, M.F., Sun, M., Liu, B.G., 2002. Platinum-group element geochemistry of the Hongge layered intrusion in the Pan-Xi area, southwestern China. *Miner. Depos.* 37, 226–239.
- Zhou, M.F., 1994. PGE distribution in 2.7-Ga layered komatiite flows from the Belingwe greenstone belt, Zimbabwe. *Chem. Geol.* 118, 155–172.
- Zhou, M.F., Sun, M., Keays, R.R., Kerrich, R., 1998. Controls on the platinum-group elemental distributions in high-Cr and high-Al chromitites: a case study of the podiform chromitites from the Chinese orogenic belts. *Geochim. Cosmochim. Acta* 62, 677–688.
- Zhou, M.F., Malpas, J., Song, X., Kennedy, A.K., Robinson, P.T., Sun, M., Leshner, C.M., Keays, R.R., 2002a. A temporal link between the Emeishan large igneous province (SW China) and the end-Guadalupian mass extinction. *Earth Planet. Sci. Lett.* 196, 113–122.
- Zhou, M.F., Yan, D.P., Kennedy, A.K., Li, Y.Q., Ding, J., 2002b. SHRIMP U–Pb zircon geochronological and geochemical evidence for Neoproterozoic arc-magmatism along the western margin of the Yangtze Block, South China. *Earth Planet. Sci. Lett.* 196, 51–67.
- Zhou, M.F., Robinson, P.T., Leshner, C.M., Keays, R.R., Zhang, C.-J., Malpas, J., 2005. Geochemistry, petrogenesis and metallogenesis of the Panzhihua gabbroic layered intrusion and associated Fe–Ti–V oxide deposits, Sichuan Province, SW China. *J. Petrol.* 46, 2253–2280.
- Zhou, M.F., Zhao, J.-H., Qi, L., Su, W.-C., Hu, R.-Z., 2006. Zircon U–Pb geochronology and elemental and Sr–Nd isotopic geochemistry of Permian mafic rocks in the Fuling area, SW China. *Contrib. Mineral. Petrol.* 151, 1–19.
- Zindler, A., Hart, S., 1986. Chemical geodynamics. *Annu. Rev. Earth Planet. Sci.* 14, 493–571.